NUREG/CR-1054

ANL-79-78

NUREG/CR-1054

ANL-79-78

TRANSITION BOILING HEAT TRANSFER IN FORCED VERTICAL FLOW

Final Report for the Period June 1978—June 1979

by

S. C. Cheng, H. Ragheb, W. W. L. Ng, K. T. Heng, S. Roy, and K. T. Poon

U of C AUA USDOE

1372 097

ARGONNE NATIONAL LABORATORY, ARGONNE, ILLINOIS

Prepared for the U. S. NUCLEAR REGULATORY COMMISSION under Interagency Agreement DOE 40-550-75

049

7911200

Available from
National Technical Information Service
Springfield, Virginia 22161

NUREG/CR-1054
ANL-79-78

Distribution
Code: R2

ARGONNE NATIONAL LABORATORY
9700 South Cass Avenue
Argonne, Illinois 60439

TRANSITION BOILING HEAT TRANSFER IN FORCED VERTICAL FLOW

Final Report for the Period
June 1978—June 1979

by

S. C. Cheng, H. Ragheb, W. W. L. Ng,
K. T. Heng, S. Roy, and K. T. Poon

Department of Mechanical Engineering
Faculty of Science and Engineering
University of Ottawa
Ottawa, Ontario, Canada

Under Contract with
Argonne National Laboratory
Subcontract No. 31-109-38-3564

June 1979

Prepared for the Systems Research Branch
Division of Reactor Safety Research
U. S. Nuclear Regulatory Commission
Washington, D. C. 20555
Under Interagency Agreement DOE 40-550-75

NRC FIN No. A2014

1372 099

TABLE OF CONTENTS

1372 100

1372 101

List of Tables

1372 102

LIST OF FIGURES

1372 103

1372 104

NOMENCLATURE

A	area
CHF	critical heat flux
c, c_p	specific heat
G	mass flux
g	solder layer thickness
H	heat content
h	heat transfer coefficient
k	thermal conductivity
k_m	mean thermal conductivity, defined in Eq. (16)
L	length of test section
n	total number of nodal points in radial direction
Q	heat transfer rate
q	heat flux (or heat transfer rate per unit area)
r	radial coordinate
T	temperature
T.C.	thermocouple
t	time
z	axial coordinate

Greek Letters

α	thermal diffusivity
Δr	radial increment
ΔT_{sub}	inlet degree of subcooling
Δt	time increment
Δz	axial increment
δ	tubing thickness
ρ	density
ϕ	boiling heat flux

Subscripts

amb	ambient
c	copper
i	nodal point index in radial direction; initial condition
in	inner wall
j	nodal point index in axial direction
n	nth nodal point in radial direction
out	outer wall
sat	saturated
t	tubing material
wm	wood's metal
z	Zircaloy

TRANSITION BOILING HEAT TRANSFER
IN FORCED VERTICAL FLOW

Final Report for the Period
June 1978—June 1979

by

S. C. Cheng, H. Ragheb, W. W. L. Ng,
K. T. Heng, S. Roy, and K. T. Poon

ABSTRACT

The study using high thermal capacity and inertia test sections to construct boiling curves for distilled water at atmospheric conditions has been continuing for the third year. In order to investigate the effect of heated surface thermal properties, boiling curves were generated from various composite test sections using one-dimensional three-layer model. A general empirical correlation including the effect of thermal properties as well as mass flux and inlet subcooling has been proposed. The earlier two-dimensional model, considering axial conduction, was modified and an application in Inconel-copper composite test section demonstrated.

An investigation for the surface wetted area during transition boiling based on the electric probe study was conducted.

I. DERIVATION OF TWO MODELS

In the earlier version of 2-D model [1,2], certain simplification was made in connection with perfect insulation assumption, e.g. Eq. (11) of [1,2]. This will be further discussed in Section I.1.1. As a result, it artificially increases the local boiling heat flux, especially near the entrance and exit of the test section. For improvement, a more realistic boundary condition will be considered here. A modified 2-D model will be derived first, followed by application in Inconel-copper composite test sections. Detailed analysis of local axial heat flux at various radial locations will also be included. Finally, a special case incorporating the solder layer effect in composite test sections, such as Zircaloy-copper test section, will be presented.

I.1 Modified Two-Dimensional Model

For the purpose of derivation, a typical composite test section and its nodal network are shown in Figs. 1 and 2. The net heat transfer Q_j from a given section j (inside the test section as shown in Fig. 2) to the fluid at time t can be expressed as the rate of change in heat content H_j of that section, plus axial conduction from neighboring sections at the same time. Note that the heat loss through the outer wall is very small, hence it can be neglected in the calculation of Q_j.

H_j can be expressed as

$$H_j(z,t) = \rho\ c\ \Delta z \int_{r_{in}}^{r_{out}} 2\pi r\ T_{i,j}\ dr \tag{1}$$

The function $T(r,z,t)$ is obtained as the solution to the two dimensional Fourier equation in cylindrical coordinates:

$$\rho c \frac{\partial T}{\partial t} = \frac{\partial}{\partial r}\left(k \frac{\partial T}{\partial r}\right) + \frac{1}{r}\left(k \frac{\partial T}{\partial r}\right) + \frac{\partial}{\partial z}\left(k \frac{\partial T}{\partial z}\right) \tag{2}$$

and is subject to the following initial and boundary conditions:

(1) $T = T(r,z,0)$ ... The initial test section temperatures are measured by the thermocouples, for simplicity, an average value is used. (3)

(2) $T(r_2, z_j) = \text{T.C. } 2,j \qquad (1 \leq j \leq 7)$ (4)

where r_2 and z_j are the coordinates of data thermocouple T.C. 2,j.

(3) $- k_c \frac{\partial T}{\partial t}\Big)_{r=r_{out}} = h(T_{n,j} - T_{amb}) \qquad (1 \leq j \leq 7)$ (5)

(4) $- k_c \frac{\partial T}{\partial z}\Big)_{z=0} = h(T_{amb} - T_{i,1}) \qquad (3 \leq i \leq n)$ (6)

(5) $- k_c \frac{\partial T}{\partial z}\Big)_{z=L} = h(T_{i,7} - T_{amb}) \qquad (3 \leq i \leq n)$ (7)

The solution of Eq. (2) can be obtained by reducing it to a system of linear first-order differential equations in t. This is achieved by discretizing along both r-direction and z-direction as shown in Fig. 2 using the approximation

$$\frac{\partial T_{i,j}}{\partial r} = \frac{T_{i+1,j}(t) - T_{i-1,j}(t)}{2\Delta r} \tag{8}$$

1372 108

$$\frac{\partial^2 T_{i,j}}{\partial r^2} = \frac{T_{i-1,j}(t) - 2T_{i,j}(t) + T_{i+1,j}(t)}{(\Delta r)^2} \tag{9}$$

and

$$\frac{\partial^2 T_{i,j}}{\partial z^2} = \frac{T_{i,j-1}(t) - 2T_{i,j}(t) + T_{i,j+1}(t)}{(\Delta z)^2} \tag{10}$$

Using Eq. (8) to (10), the following system of equations can be inferred from Eq. (2).

$$\frac{d\,T_{i,j}}{dt} = \alpha_c\left[\frac{T_{i-1,j} - 2T_{i,j} + T_{i+1,j}}{(\Delta r)^2}\right] + \frac{\alpha_c}{r_i}\left(\frac{T_{i+1,j} - T_{i-1,j}}{2\Delta r}\right)$$

$$+ \alpha_c\left[\frac{T_{i,j-1} - 2T_{i,j} + T_{i,j+1}}{(\Delta z)^2}\right] \tag{11}$$

$$(3 \le i \le n;\ 1 \le j \le 7)$$

where

$$r_i = r_{in} + \delta + (i - 2)\Delta r$$

The three boundary conditions, Eq. (5) to (7), can also be discretized in the following forms:

$$-\frac{k_c}{2}\left(\frac{T_{n,j} - T_{n-1,z}}{\Delta r} + \frac{T_{n+1,j} - T_{n,j}}{\Delta r}\right) = h(T_{n,j} - T_{amb}) \tag{12}$$

$$(1 \le j \le 7)$$

$$-\frac{k_c}{2}\left(\frac{T_{i,2} - T_{i,1}}{\Delta z} + \frac{T_{i,1} - T_{i,0}}{\Delta z}\right) = h(T_{amb} - T_{i,1}) \tag{13}$$

$$(3 \le i \le n)$$

$$-\frac{k_c}{2}\left(\frac{T_{i,7} - T_{i,6}}{\Delta z} + \frac{T_{i,8} - T_{i,7}}{\Delta z}\right) = h(T_{i,7} - T_{amb}) \tag{14}$$

$$(3 \le i \le n)$$

The imaginary temperatures $T_{n+1,j}$, $T_{i,0}$ and $T_{i,8}$ in Eq. (11) can be eliminated by using Eqs. (12), (13) and (14).

1372 109

Eq. (11) contains a system of 7x(n-2) equations with the same number of unknowns in $T_{i,j}$ $(3 \le i \le n;\ 1 \le j \le 7)$. Once $T_{i,j}$ have been solved and $dT_{2,j}/dt$ determined from experimental data, the inner wall temperature $T_{1,j}$ can then be calculated in the following Fourier equation based on the nodal point (2,j)

$$\frac{\left[r_2^2 - (r_2 - \frac{\delta}{2})^2\right] \rho_t c_t + \left[(r_2 + \frac{\Delta r}{2})^2 - r_2^2\right]\rho_c c_c}{(r_2 + \frac{\Delta r}{2})^2 - (r_2 - \frac{\delta}{2})^2} \frac{dT_{2,j}}{dt}$$

$$= \frac{k_c \frac{T_{3,j} - T_{2,j}}{\Delta r} - k_t \frac{T_{2,j} - T_{1,j}}{\delta}}{\frac{1}{2}(\Delta r + \delta)} + \frac{1}{r_2} \frac{1}{2} \left(k_c \frac{T_{3,j} - T_{2,j}}{\Delta r} + k_t \frac{T_{2,j} - T_{1,j}}{\delta}\right)$$

$$+ k_m \left[\frac{T_{2,j-1} - 2T_{2,j} + T_{2,j+1}}{(\Delta z)^2}\right] \qquad (1 \le j \le 7) \qquad (15)$$

where $$k_m = k_t \frac{\left[r_2^2 - (r_2 - \frac{\delta}{2})^2\right]}{(r_2 + \frac{\Delta r}{2})^2 - (r_2 - \frac{\delta}{2})^2} + k_c \frac{\left[(r_2 + \frac{\Delta r}{2})^2 - r_2^2\right]}{(r_2 + \frac{\Delta r}{2})^2 - (r_2 - \frac{\delta}{2})^2} \qquad (16)$$

Eq. (16) is the expression of mean thermal conductivity based on the Ohm's law in laminae parallel. In solving Eq. (15), $T_{2,0}$ and $T_{2,8}$ are needed. Since these temperatures are not available, they can be extrapolated from three neighbouring interior nodal points in the z-direction.

Eq. (1), expressed in terms of summation, becomes

$$H_j = 2\pi\Delta z \left[0.5\, T_{1,j}\, r_{in}\, \delta\rho_t c_t + 0.5\, T_{2,j}(r_{in} + \delta)\delta\, \rho_t c_t \right.$$

$$\left. + 0.5\, T_{2,j}(r_{in} + \delta)\Delta r\, \rho_c c_c + \left(\sum_{i=3}^{n-1} T_{i,j}\, r_i\, \Delta r\, \rho_c c_c\right) + 0.5\, T_{n,j}\, r_n \Delta r\, \rho_c c_c\right] \qquad (17)$$

1372 110

The expression of net heat flux q_j (based on inner wall area) from section j through plane j to the fluid in terms of H_j and axial conduction is:

$$q_j = \frac{1}{A_{in}}\left(- \frac{dH_j}{dt} + Q_{j+1,j} - Q_{j,j-1}\right)$$

$$= \frac{1}{2\pi r_{in}\Delta z}\left(- \frac{dH_j}{dt} + Q_{j+1,j} - Q_{j,j-1}\right) \tag{18}$$

where $Q_{j+1,j}$ the axial conduction from section $j + 1$ to section j, can be expressed as

$$Q_{j+1,j} = \frac{2\pi}{\Delta z}\Big[0.5\, r_{in}\, \delta k_t(T_{1,j+1} - T_{1,j}) + 0.5(r_{in} + \delta)\delta k_t(T_{2,j+1} - T_{2,j})$$

$$+ 0.5(r_{in} + \delta)\, \Delta r\, k_c(T_{2,j+1} - T_{2,j}) + \sum_{i=3}^{n-1} r_i \Delta r\, k_c(T_{i,j+1} - T_{i,j})$$

$$+ 0.5\, r_n\, \Delta r\, k_c(T_{n,j+1} - T_{n,j})\Big] \tag{19}$$

$Q_{j,j-1}$ can be obtained in a similar manner.

The net heat flux q_j can be approximated by

$$q_j \doteq k_t\, \frac{T_{2,j} - T_{1,j}}{\delta} \tag{20}$$

It has been found that q_j calculated from Eq. (20) in general results in less than 10% error compared to that of Eq.(18).

1372 111

I.1.1 Application in Inconel-Copper Composite Test Sections

A typical Inconel-copper composite test section is shown in Fig. 1 and its nodal network is shown in Fig. 2. Since T.C. 2,1 and T.C. 2,7 are not available, it has to rely on approximate values. After studying the trend of axial data thermocouple temperature distribution [1,3], one can estimate T.C. 2,1 by extrapolation from three interior points (T.C. 2,2, T.C. 2,3 and T.C. 2,4). T.C. 2,7 can be obtained in a similar fashion. Because of this approximation, it is more reasonable to obtain $T_{1,1}$ and $T_{1,7}$ by extrapolating from three axial interior points instead of Eq. (15). It is believed that all these extrapolations may affect slightly the resultant boiling curves on plane 1 and 7. This definitely is a vast improvement over the earlier model [1,2] which assumed $T_{i,1} = T_{i,2}$ and $T_{i,6} = T_{i,7}$ $(1 \leq i \leq n)$ (implying T.C. 2,1 = T.C. 2,2 and T.C. 2,6 = T.C. 2,7) in connection with perfect insulation assumption.

All calculations were performed via CSMP computer package. The Runge-Kutta fixed-step size method has been used in numerical integration with selection of $n = 9$ and $\Delta t = 0.1$ sec and its convergency checked. NLFGEN function generation (non-linear function generation) capability of CSMP was used to generate $T_{2,j}$ from measured data and DERIV (derivative) module used to compute $dT_{2,j}/dt$ from $T_{2,j}$ and dH_j/dt from H_j. The heat transfer coefficient h

1372 112

was set equal to 18 $W/m^2 {}^oC$ which has been determined experimentally under a no-flow condition. All the thermal properties used in this report are presented in Table I.

A typical set of boiling curves for a mass flux of 136 kg/m^2s and an inlet subcooling of 13.9^{o}C from 1500 run series was constructed using the modified 2-D analysis as shown in Fig. 3. For obvious reasons, plane 1 and 7 boiling curves are not shown. A large spread in boiling curves is noticed for the 2-D analysis. However, the spread is somewhat reduced in comparison with the results of earlier model [1,3]. This is due to the removal of the simplification associated with perfect insulation assumption. The higher values of boiling curves on plane 2 and 3 are attributed to (a) lower bulk fluid temperature, (b) thermal boundary layer not being fully established, and (c) end effects. Other discussion of the 2-D and 1-D results is presented in [1,2,3], and will not be repeated here.

In order to gain some insight into axial conduction, the local axial heat flux will be analyzed. The local axial heat flux at nodal point (i,j) from section $j + 1$ to section j can be expressed as

$$q_{j+1,j(i)} = k \frac{T_{i,j+1} - T_{i,j}}{\Delta z} \tag{21}$$

and similarly, $q_{j,j-1(i)}$ becomes

$$q_{j,j-1(i)} = k \frac{T_{i,j} - T_{i,j-1}}{\Delta z} \tag{22}$$

For the purpose of comparison, the average local radial heat flux at nodal point (i,j) can be defined and written as

$$\frac{1}{2}\left(q_{i+1,\, i(j)} + q_{i,i-1(j)}\right) = \frac{1}{2}\left(k\,\frac{T_{i+1,j} - T_{i,j}}{\Delta r} + k\,\frac{T_{i,j} - T_{i-1,j}}{\Delta r}\right) \quad (3 \le i \le n) \qquad (23a)$$

$$\frac{1}{2}\left(q_{i+1,i(j)} + q_{i,i-1(j)}\right) = \frac{1}{2}\left(k\,\frac{T_{i+1,j} - T_{i,j}}{\Delta r} + k\,\frac{T_{i,j} - T_{i-1,j}}{\delta}\right) \quad (i = 2) \qquad (23b)$$

Fig. 4 presents the local axial heat flux at the mid-section at 185 sec and 213 sec, and the average local radial heat flux is also included for comparison. At 185 sec, the corresponding wall temperature is 284°C which represents a typical state in transition boiling régime (see plane 4 boiling curve in Fig. 3). Whereas, at 213 sec, the corresponding wall temperature is 200°C which is very close to CHF. Additional local axial heat flux at 108 sec ($T_w = 367°C$) and 199 sec ($T_w = 258°C$) is presented in Fig. 5. Following observations referring to the mid-section (Figs. 4 and 5), can be made:

(a) The local axial heat flux from above ($q_{j+1,j(i)}$) and below ($q_{j,j-1(i)}$) at 185 sec is approximately the same as that at 213 sec. This, in fact, is the case for the most transition boiling régime covering the wall temperature between 320°C and CHF. Above 320°C, the local axial heat flux is smaller. At all times, the minimum local axial heat flux occurs at nodal point 1 due to low thermal conductivity of tubing material, whereas, the highest local axial heat flux occurs at nodal point 2.

(b) At 185 sec, the net local axial heat flux is relatively large in comparison with the average local radial heat flux especially at the nodal points 2 and 3. Whereas, at the nodal point 1, the net local axial heat flux is relatively small by virtue of low thermal conductivity value of tubing material.

(c) At 213 sec, the net local axial heat flux is relatively small in comparison with the average local radial heat flux.

I.2 One Dimensional Three-Layer Model

For certain types of composite test sections, e.g. Zircaloy-copper test sections, due to problems in brazing copper to Zircaloy, a liquid metal gland (wood's metal) was used instead to provide good thermal contact between the two materials as shown in Fig. 6. Note that wood's metal is in the liquid state (melting point 70^{o}C) at test conditions. It is, therefore, suspected that the data thermocouple T.C. 1 (Fig. 6), may not be maintained at the interface position of the tube and wood's metal. As a result, a new thermocouple T.C. 2 was used for the data thermocouple in this application. T.C. 2 is located on the copper side, but very close to the interface of wood's metal and copper. It was found out later that the temperature measured at T.C. 1 location, is much higher than that predicted. This is to confirm the earlier suspicion about the measurement of T.C. 1.

For simplicity, the 1-D model (two-layer) [4], after some modification was used in data reduction. Because of the location of the new data thermocouple T.C. 2, the low value of thermal conductivity of wood's metal (Table I) and its thickness (almost three times thicker than silver solder), the effect of solder layer has to be included in the analysis. The derivation for 1-D three layer analysis in this case is essential, the same as that of 2-D case, except two extrapolations (based on Fourier equation) are required to determine the inner wall temperature.

For 1-D model, the Fourier equation on the copper side can be obtained from Eq. (11) after neglecting axial conduction

$$\frac{dT_i}{dt} = \alpha_c \left[\frac{T_{i-1} - 2T_i + T_{i+1}}{(\Delta r)^2} \right] + \frac{\alpha_c}{r_i} \left(\frac{T_{i+1} - T_{i-1}}{2\Delta r} \right) \qquad (24)$$

$$(3 \leq i \leq n)$$

where

$$r_i = r_{in} + \delta + g + (i-2)\, \Delta r$$

and

$$-\frac{k_c}{2} \left(\frac{T_n - T_{n-1}}{\Delta r} + \frac{T_{n+1} - T_n}{\Delta r} \right) = h(T_n - T_{amb}) \qquad (25)$$

where Eq. (25) is the boundary condition at the outer wall of the test section. All the symbols in this derivation are referred to Fig. 6.

Equation (24) contains a system of n-2 equations with n-2 unknowns in $T_i (3 \le i \le n)$, where T_{n+1} in the equation is to be eliminated from Eq. (25). With T_i available and dT_2/dt determined from experimental data, T_1 can be calculated from the Fourier equation based on the nodal point 2

$$\frac{\left[r_2^2 - (r_2 - \frac{g}{2})^2\right] \rho_{wm} c_{wm} + \left[(r_2 + \frac{\Delta r}{2})^2 - r_2^2\right]\rho_c c_c}{(r_2 + \frac{\Delta r}{2})^2 - (r_2 - \frac{g}{2})^2} \frac{dT_2}{dt}$$

$$= \frac{k_c \frac{T_3 - T_2}{\Delta r} - k_{wm} \frac{T_2 - T_1}{g}}{\frac{1}{2}(\Delta r + g)} + \frac{1}{r_2}\frac{1}{2}\left(k_c \frac{T_3 - T_2}{\Delta r} + k_{wm} \frac{T_2 - T_1}{g}\right) \quad (26)$$

With T_1 known and from which dT_1/dt determined, the inner wall temperature T_o can then be computed from the Fourier equation based on the nodal point 1

$$\frac{\left[r_1^2 - (r_1 - \frac{\delta}{2})^2\right]\rho_z c_z + \left[(r_1 + \frac{g}{2})^2 - r_1^2\right]\rho_{wm} c_{wm}}{(r_1 + \frac{g}{2})^2 - (r_1 - \frac{\delta}{2})^2} \frac{dT_1}{dt}$$

$$= \frac{k_{wm} \frac{T_2 - T_1}{g} - k_z \frac{T_1 - T_0}{\delta}}{\frac{1}{2}(g + \delta)} + \frac{1}{r_1}\frac{1}{2}\left(k_{wm} \frac{T_2 - T_1}{g} + k_z \frac{T_1 - T_0}{\delta}\right) \quad (27)$$

where

$$r_1 = r_{in} + \delta.$$

1372 117

Finally, the heat content of the test section H and the average heat flux q to the fluid can be expressed as

$$H = 2\pi L\Big[0.5\ T_0 r_{in}\delta\rho_z c_z + 0.5\ T_1(r_{in} + \delta)\delta\rho_z c_z + 0.5\ T_1(r_{in} + \delta)g\rho_{wm}c_{wm}$$
$$+ 0.5\ T_2(r_{in} + \delta + g)g\rho_{wm}c_{wm} + 0.5\ T_2(r_{in} + \delta + g)\Delta r\rho_c c_c + \Big(\sum_{i=3}^{n-1} T_i r_i \Delta r \rho_c c_c\Big)$$
$$+ 0.5\ T_n r_n \Delta r \rho_c c_c\Big] \qquad (28)$$

and

$$q = -\frac{1}{2\pi r_{in} L}\frac{dH}{dt} \qquad (29)$$

1372 118

II. EXPERIMENTAL RESULTS FOR COMPOSITE TEST SECTIONS

During this report period eleven run series for composite test sections were conducted, the specifications of test sections and highlights of these run series are described in Table II and their thermal properties used in calculations presented in Table I. Most run series were analyzed via 1-D three-layer model using wood's metal as a solder.

II.1 1600 Run Series (Inconel-copper) [5]

The Inconel-copper test section in 1600 series was specifically constructed for steady-state operation. To ensure the boiling curve covering the full range, more heaters with higher power rating were used. The detailed test section configuration and controlling methods are described in [6,7] and [6] appears in APPENDIX I. As seen from Fig. 2, in Appendix I, good agreement between the transient and steady-state results in film and transition boiling is observed. However, it is noticed that the transient boiling curve in nucleate boiling is shifted to higher wall temperatures. This is possibly due to bubble clouding on the heated surface during quenching experiments thus retarding the boiling heat transfer process. Since our earlier copper transient and steady-state data in nucleate boiling showed good agreement, thus it is suspected that the bubble clouding may depend on the thermal properties of heating surface in general and more specially depend on the thermal conductivity.

II.2 1700 and 1800 Run Series (Zircaloy-copper) [5,8]

These are first two Zircaloy-copper composite test sections using wood's metal for soldering with a solder layer being 0.0178 cm for 1700 run series and 0.025 cm for 1800 run series. Because of problems in brazing copper to Zircaloy, wood's metal was used instead to provide good thermal contact between the two materials. The schematic diagram for the test section is shown in Fig. 7. To ensure that no air was trapped when filling the gap, three evenly spaced vents were drilled at the bottom of the test section for allowing air to escape. These vents were plugged during the tests. At the top of the test section, a recess containing an excess quantity of wood's metal was provided to compensate for any possible leak of wood's metal. A cylindrical enclosure was placed on the top of test section with argon gas blown inside to minimize oxidation on the surface of wood's metal in the recess during experiments.

Many different schemes were attempted in data reduction to construct boiling curves using T.C. 1 or T.C. 2 as data thermocouple (Fig. 7). At this time, 1-D three-layer model was not developed yet. Some of these tries are shown in Fig. 8. All three boiling curves in Fig. 8 show a similar trend. The boiling curve I was constructed using 1-D two-layer analysis (assuming $k_{wm} = k_c$) with T.C. 1 as data thermocouple; the boiling curve II was constructed in a same way except k_{wm} value being lumped into k_c. Whereas, the boiling curve III was obtained again via 1-D two-layer analysis, but using

T.C. 2 as data thermocouple instead with k_{wm} value being lumped into k_z.

The difficulties associated with data reduction in these series can be attributed to:

(1) Wood's metal melts (melting point $70^{o}C$) at the test temperature range, in addition, during this range, the value of k could vary from 25-50 $W/m^{o}C$.

(2) The existence of contact resistance when using wood's metal as a solder has been found in a separate experiment. Unfortunately, this experimental result is only valid for the test section temperature at about $100^{o}C$ and, therefore, it cannot be generalized to cover the entire test temperature range. The presence of contact resistance is thought to be due to (a) wetting character between Zircaloy surface and wood's metal, (b) transition of phase change for wood's metal, (c) violent shaking of test section, especially near CHF, this shaking may possibly prevent the liquid wood's metal from completely filling the gap, and (d) oxidation due to trapped air.

(3) Because of the conditions described in (2), it is doubtful that T.C. 1 can be maintained at close contact on the outer Zircaloy tube as originally assumed.

In light of the aforementioned uncertainties, (a) the lower limit of k value of wood's metal is adopted in the analysis to offset the contact resistance, and (b) T.C. 2 is chosen as data T.C. instead of T.C. 1. As a result, the 1-D three-layer analysis drived in Section I.2 is required in data reduction.

Fig. 9 presents boiling curves for $\Delta T_{sub} = 13.9^{o}C$ with $G = 68$, 136 and 203 kg/m^2s. Note that CHF's are lower, T_{CHF}'s higher and the minimum heat flux points unchanged in comparison with those of Inconel-copper 1500 run series under the same flow conditions. Another family of boiling curves for $\Delta T_{sub} = 0^{o}C$, as illustrated in Fig. 10, shows a similar trend.

A simulation run was attempted to see the effect of a higher value of k for wood's metal. Using $k = 50\ W/m^{o}C$, the resultant boiling curve shows little change with the exception that T_{CHF} occurs at $8^{o}C$ higher wall temperature.

II.3 1900 Run Series (Inconel-copper) [9].

The purpose of this silver soldered test section was to compare the boiling curves generated using three-layer and two-layer analyses via T.C. 2 and T.C. 1 (Fig. 7), respectively. It has been found that the resultant boiling curves based on these analyses give good agreement as shown in Fig. 11. However, the overall boiling curves are somewhat lower than those of 1500 run series. This is because the test section was soldered first by wood's metal to study the effect of wood's metal soldering on resultant boiling curves. After that, it was cleaned and resoldered by silver solder, as a result, due possibly to some residual wood's metal or changing surface conditions, it could not reproduce 1500 run series results.

Note that T.C. 1 is located at the interface between the tube and solder and it remains there under the test conditions due to silver soldering. This may not be true in the case of wood's metal soldering. Thus, it is concluded that whenever wood's metal is used as a solder, the 1-D three-layer analysis will be employed with T.C. 2 as the data thermocouple.

II.4 2000 Run Series (Zircaloy-copper) [9].

The "shrink fit" method was attempted in constructing this test section with the bore inside the copper block being 0.0152 cm smaller than the tube diameter. The copper block temperature was raised to a "red hot" condition (650^{o}C) in a cylindrical enclosure with argon gas circulated inside, before forced fitting. Apparently, due to severe oxidation on Zircaloy surface and subsequent scale built up, no quenching was observed in the ensuing experiments.

II.5 2100 Run Series (Zircaloy-copper) [9]

This is the third wood's metal soldered Zircaloy-copper composite test section with a solder layer of 0.0356 cm. It was found out in Section II.6 that the gap size of 0.0356 cm is the optimum one in minimizing contact resistance. Nine complete runs were obtained; Fig. 12 shows the effect of subcooling, whereas the effect of mass flux is presented in Fig. 13. Note that the overall boiling curves in this series are higher than those of 1700 run series, in which the gap size of 0.0178 cm was used.

II.6 2200 and 2400 Run Series (Inconel-copper) [9].

These two test sections were constructed to study the effect of wood's metal soldering and to find out the optimum gap size of solder. The gap size is 0.0533 cm for 2200 run series test section and 0.0356 cm for 2400 run series test section. Comparing boiling curves among these two series and 1900 run series, it seems that the 2400 run series gives the highest overall boiling curves. Thus, the gap size of 0.0356 cm apparently is the optimum value in yielding minimum contact resistance. The boiling curve for 2400 run series is shown in Fig. 14.

II.7 2300 Run Series (Aluminum-copper) [9].

II.8 2500 Run Series (Copper-copper) [9].

These two composite test sections were constructed to study the effect of aluminum and copper heated surfaces using wood's metal solder on boiling curves with the gap size of 0.0356 cm. Their boiling curves are presented in Fig. 14. Due to high value of thermal conductivity for both aluminum and copper, severe heat losses were incurred at the piping connections. Separate heat

1372 124

losses tests were conducted at no-flow conditions. The boiling curves presented in Fig. 14 have been corrected by subtracting the heat losses.

II.9 2700 Run Series (Brass-copper)

At this time, it was evident that wood's metal soldered composite test sections could not produce satisfactory boiling curves due to solder contact resistance. In order to see the effect of thermal properties on boiling curves, a new material such as brass, which can be silver soldered, was tested. A family of boiling curves for a constant $\Delta T_{sub} = 13.6^{0}C$, is illustrated in Fig. 15.

II.10 Conclusions and Discussion

1. Good agreement has been observed between transient and steady-state data for silver soldered Inconel-copper test section (1600 run series) especially in the transition boiling regime.
2. For wood's metal soldered composite test sections, the optimum gap size is 0.0356 in minimizing the effect of contact resistance.
3. For wood's metal soldered composite test sections, the 1-D three-layer analysis using T.C. 2 as data thermocouple to construct boiling curves proves to be most satisfactory.
4. A comparison for thermocouple signals from silver soldered Inconel-copper composite test section and wood's metal soldered Inconel-copper composite test section under same flow conditions is shown in Fig. 16. A large fluctuation of thermocouple signal at high heat flux region up to CHF for wood's metal soldered

test section is observed. Apparently, the contact resistance impedes the supply of heat flow from neighbouring material, thus causing a large, temporary local temperature drop. It then requires some time to recover the temperature before cooldown can be continued.

5. In light of 4., the boiling curves generated from wood's metal soldered test section do not anticipate to have good agreement with those of silver soldered results. This, in fact, is the case as shown in Fig. 17. For comparison, the boiling curve produced from wood's metal soldered copper-copper test section is also shown in Fig. 17 along with that of copper block data. Again, large discrepancy between these two boiling curves is observed.

6. Fig. 14 shows the comparison of boiling curves for four different heated surfaces, namely, Zircaloy, aluminum, Inconel and copper, all using wood's metal solder with a constant thickness of 0.0356 cm. This provides some qualitative observation on the effects of thermal properties on boiling curves, i.e.,

   (a) The boiling curve on Zircaloy surface is very similar to that on Inconel surface, this is expected as both materials have the similar value of k. The same conclusion can be drawn on aluminium and copper surfaces.

   (b) The rewet temperature is dependent on the value of k of a heated surface -- the higher the value of k the lower the rewet temperature.

1372 126

(c) All four boiling curves give the same value of CHF, whereas T_{CHF} shows a slight decrease with increasing k.

(d) The ρc_p effect on the boiling curves is not clear since it never changes more than one order of magnitude among these four materials tested. However, it is believed that ρc_p will influence the boiling curves in the same way as k .

7. Based on the findings of 6., the boiling curves on Zircaloy surface can be approximated by those of Inconel surface through 1500 run series.
8. The results for brass-copper composite test section will be discussed in the next section (III. CORRELATIONS).
9. A comparison of 1500 run series data with the correlations of Hsu [10], Ramu and Weisman [11], and Tong [12], is shown in Fig. 18. Hsu's correlation seems to give the best prediction.
10. Work has been continuing on the electric probe studies. A recent development involving the fraction of surface wetted area during transition boiling is presented in APPENDIX II [13].

1372 127

III. CORRELATIONS

Most of the correlation studies up to this point has been concentrated on empirical correlations due to simplicity. Two separate empirical correlations for copper surface and Inconel surface have been completed. A general empirical correlation including the effect of thermal properties has been proposed.

III.1 Copper Empirical Correlation [5]

An empirical correlation based on 500 run series copper test section data [1] has been developed as follows:

$$\phi = 6.565 \times 10^{8}(\Delta T_{sat})^{-1.71788} \exp(0.0177\ \Delta T_{sub} + 0.00571\ G) \quad (30)$$

This correlation was derived based on 225 data points from nine experimental runs with an rms error of 8.7%. A typical comparison is shown in Fig. 19.

III.2 Inconel Empirical Correlation [5]

An empirical correlation based on 1500 run series Inconel-copper composite test section data [1] has been developed as follows:

$$\phi = 0.820[5266.6(\Delta T_{sat})^{0.75} + 107910.0\ \Delta T_{sat} \exp(-0.025\ \Delta T_{sat})] \cdot$$

$$\exp[(0.0045\ \Delta T_{sub} + 0.0005\ G)\ln \Delta T_{sat}] \quad (31)$$

This correlation was derived based on 425 data points from nine experimental runs with an rms error of 9.7%. A typical comparison is shown in Fig. 20.

1372 128

III.3 Development of General Empirical Correlation

In order to develop a general empirical correlation including the effect of $k\rho c_p$, boiling curves on at least three different heated surfaces are required. Boiling curves on copper surface (500 run series) and Inconel surface (1500 run series) were available. All wood's metal soldered test sections data at best can only provide some qualitative effect of $k\rho c_p$ on boiling curves, therefore, they cannot be used for correlation purposes. This prompts the construction of brass-copper composite test section (2700 series). Unfortunately, brass cannot be silver soldered with copper as well as Inconel with copper. This casts some doubt about the results. A brass block test section arrangement similar to that of 500 copper run series seems worth trying at this point.

III.3.1 2800 Run Series (Brass block)

This test section is exactly the same as that of 500 copper run series using the bracket arrangement to minimize axial heat loss through both ends of the test section connections. A typical family of boiling curves for a constant of $\Delta T_{sub} = 13.9^oC$ is shown in Fig. 21. Note that some large drops of boiling curves occur. It is believed that this is associated with the low value of thermal conductivity of brass block. Fortunately, these drops occur at different wall temperatures for a fixed flow condition run. In other words, several repeated runs are required to construct a complete boiling curve under a given flow condition. For high inlet subcooling and high mass flux conditions, only partial transition boiling curves are obtainable.

III.3.2 2900 Run Series (Brass block)

This test section was constructed to produce steady-state data. Work is still in progress, however, preliminary results show that it agrees well with those of transient data from 2800 run series.

III.3.3 General Empirical Correlation

Fig. 22 shows the effect of $k\rho c_p$ on boiling curves. It is apparently that the transition boiling curves shift upwards and towards the right with a decrease value of $k\rho c_p$. This is consistent with the findings of wood's metal soldered test sections (Fig. 14). With this in mind, the following preliminary general empirical correlation has been proposed:

$$\phi = 9.267\times10^{7}(\Delta T_{sat})^{-1.18910-0.22599\times10^{-5}\sqrt{k\rho c_p}}\ \exp(0.02012\ \Delta T_{sub} + 0.00393\cdot G + \frac{5770}{\sqrt{k\rho c_p}}) \qquad (32)$$

This correlation was derived based on 601 data points with an rms error of 12.65%. It consists of 225 points from 500 copper run series, 223 points from 1500 Inconel-copper run series and 153 points from 2800 brass run series. Three different families of boiling curves corresponding to three different heated surfaces appear in Fig. 23 to 25.

III.4 Conclusions and Discussion

1. All three empirical correlations show good agreement with experimental data. Continuous refinement for the general empirical correlation undoubtedly will be required as more experimental data become available.
2. An empirical correlation based on local equilibrium quality rather than inlet subcooling is under investigation. It was felt that this approach may be more useful in practical applications.
3. The rewetting for a lower $k\rho c_p$ material such as Inconel occurs at a higher wall temperature as illustrated in Fig. 22. This can be explained from the cold spot concept. The cold spot is formed due to liquid droplets evaporating upon collision with wall and is thus associated with a momentary temperature drop. For a lower $k\rho c_p$ material, this sudden local temperature drop can be quickly recovered only at a higher wall temperature. Otherwise, the cold spot will take hold and start spreading to initiate rewetting. Conversely, for a higher $k\rho c_p$ material, it can prevent the establishing and spreading of cold spot at a lower wall temperature. Henry [14], and Yao and Henry [15], found that for a lower $k\rho c_p$ material, a higher minimum film boiling temperature is required to sustain stable film boiling.
4. A phenomenological approach starting from CHF would give a more general and perhaps more accurate correlation, but the task is certainly a very difficult one to say the least.

1372 131

IV. RECOMMENDATION FOR FUTURE WORK

In the next twelve-month period, the following aspects of the studies will be conducted:

1. To refine the general empirical correlation, and to derive a phenomenological correlation;
2. To produce boiling curves under slightly pressurized conditions (< 200 psia), a proposed system is shown in Fig. 26;
3. To continue the work on electric probes.

ACKNOWLEDGEMENTS

The authors wish to express their gratitude to the Nuclear Regulatory Commission for providing the financial support for this project and the Argonne National Laboratory for their administration. The authors are greatly indebted to Dr. D.C. Groeneveld, AECL, for his technical advice and Drs. Y.Y. Hsu, NRC, and P.A. Lottes, ANL, for their valuable suggestions and coordination throughout the investigation.

REFERENCES

1. Cheng, S.C., Ragheb, H., Ng, W.W.L., Heng, K.T. and Roy, S., "Transition Boiling Heat Transfer in Forced Vertical Flow", NUREG/CR-0357 and ANR-78-75, Final Report (1977-78), Argonne Contract No. 31-109-38-3564, June 1978.

2. Cheng, S.C., "Transition Boiling Curves Generated From Quenching Experiments Using a Two-Dimensional Model", Lett. Heat Mass Transfer, Vol. 5, 1978, pp. 391-403.

3. Cheng, S.C. and Ragheb, H., "Transition Boiling Data of Water on Inconel Surface Under Forced Convective Conditions", Int. J. Multiphase Flow (in press).

4. Cheng, S.C., Heng, K.T. and Ng, W.W.L., "A Technique to Construct a Boiling Curve from Quenching Data Considering Heat Loss", Int. J. Multiphase Flow, Vol. 3, 1977, pp. 495-499.

5. Cheng, S.C., etc., "Transition Boiling Heat Transfer in Forced Vertical Flow", Quarterly Report No. 9 (July-September 1978), Argonne Contract No. 31-109-38-3564, September 1978.

6. Ng, W.W.L. and Cheng, S.C., "Steady State Flow Boiling Curve Measurements Via Temperature Controllers", Lett. Heat Mass Transfer, Vol. 6, 1979, pp. 77-81.

7. Ng, W.W.L., "Transition Boiling Heat Transfer in Forced Vertical Flow Via High Thermal Capacity Composite Test-Section Using Steady State Method", Lett. Heat Mass Transfer, Vol. 5, 1978, pp. 405-411.

8. Cheng, S.C., etc., "Transition Boiling Heat Transfer in Forced Vertical Flow", Quarterly Report No. 10 (October-December 1978), Argonne Contract No. 31-109-38-3564, December 1978.

9. Cheng, S.C., etc., "Transition Boiling Heat Transfer in Forced Vertical Flow", Quarterly Report No. 11 (January-March 1978), Argonne Contract No. 31-109-38-3564, March 1979.

10. Hsu, Y.Y., "Tentative Correlation of Reflood Heat Transfer", presented at the Third Water Reactor Safety Information Meeting, Germantown, Maryland, 1975.

11. Ramu, K. and Weisman, J., "A Method for the Correlation of Transition Boiling Heat Transfer Data", Proceedings of Fifth International Heat Transfer Conference, Tokyo, Vol. IV, pp. 160-164, Paper B4.4, 1974.

12. Tong, L.S., "Heat-Transfer Mechanisms in Nucleate and Film Boiling", Nucl. Eng. and Design Vol. 21, pp. 1-25, 1972.

13. Ragheb, H.B. and Cheng, S.C., "Surface Wetted Area During Transition Boiling in Forced Convective Flow", J. of Heat Transfer Vol. 101, 1979, pp. 381-383.

14. Henry, R.E., "A Correlation for the Minimum Film Boiling Temperature", AIChE Symp. Series No. 138, Vol. 70, 1974, pp. 81-90.

15. Yao, S.C. and Henry, R.E., "An Investigation of the Minimum Film Boiling Temperature on Horizontal Surfaces", J. Heat Transfer, Vo. 100, 1978, pp. 260-267.

1372 134

TABLE I Thermal Properties of Heated Surfaces & Solders

Heated Surface	k (W /m°C)	ρ (kg/m³)	c_p (J/kg°C)
Copper	379	8938	385
Inconel	17	8169	435
Zircaloy	15	6549	316
Aluminium	229	2707	896
Brass (70% cu, 30% Zn)	144	8522	385
Solder			
Silver solder	50	8938 *	385 *
Wood's metal	25 **	9134	145 **

* Assuming the property of copper

** Approximate value

Table II Composite Test Sections

Run Series	Tubing Material	Tubing Dimension	Solder	Comment
1600	Inconel	O.D. = 1.27 cm δ = 0.038 cm g = 0.013 cm	Silver solder	24 heaters with 250 W to each; used for both steady state and transient runs
1700 & 1800	Zircaloy	O.D. = 1.31 cm δ = 0.0559 cm g = 0.0178 cm for 1700 series g = 0.025 cm for 1800 series	Wood's metal	Using 1-D two-layer and three-layer analyses
1900	Inconel	O.D. = 1.27 cm δ = 0.038 cm g = 0.0178 cm	Silver solder	To compare the results of two-layer and three-layer analyses using silver solder
2000	Zircaloy	O.D. = 1.31 cm δ = 0.0559 cm		Using "shrink fit" with the bore inside the copper block being 0.0152 cm smaller than O.D. of tube.
2100	Zircaloy	O.D. = 1.31 cm δ = 0.0559 cm g = 0.0356 cm	Wood's metal	Using 1-D three-layer analysis
2200 & 2400	Inconel	O.D. = 1.27 cm δ = 0.038 cm g = 0.0533 cm for 2200 series g = 0.0356 cm for 2400 series	Wood's metal	Using 1-D three-layer analysis
2300	Aluminum	O.D. = 1.40 cm δ = 0.0635 cm g = 0.0356 cm	Wood's metal	Using 1-D three-layer analysis
2500	Copper	O.D. = 1.27 cm δ = 0.038 cm g = 0.0356 cm	Wood's metal	Using 1-D three-layer analysis
2700	Brass	O.D. = 1.27 cm δ = 0.038 cm g = 0.013 cm	Silver solder	Using 1-D two-layer analysis

1372 136

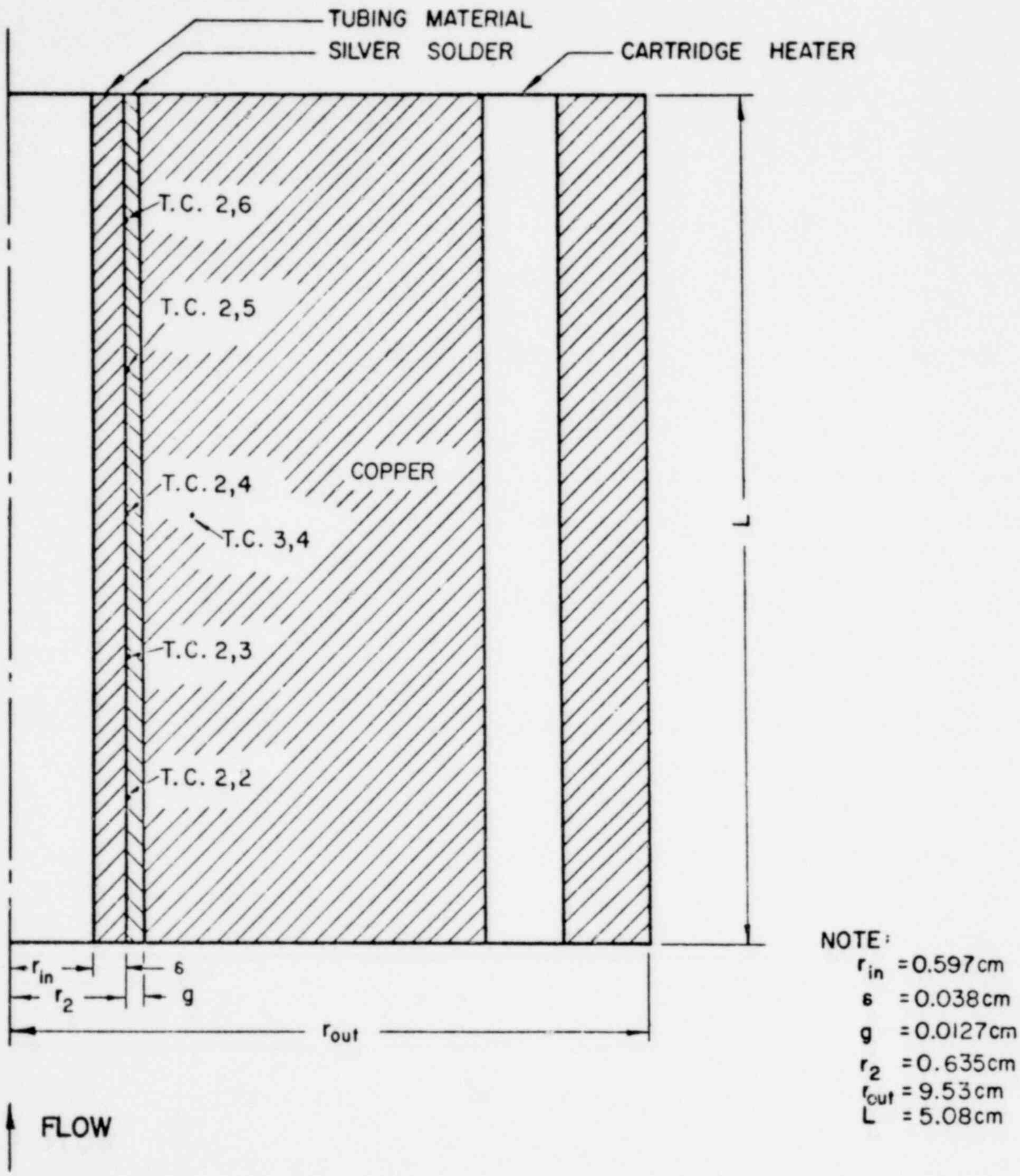

Fig. 1. Location of Thermocouples in Inconel-Copper Composite Test Section

1372 137

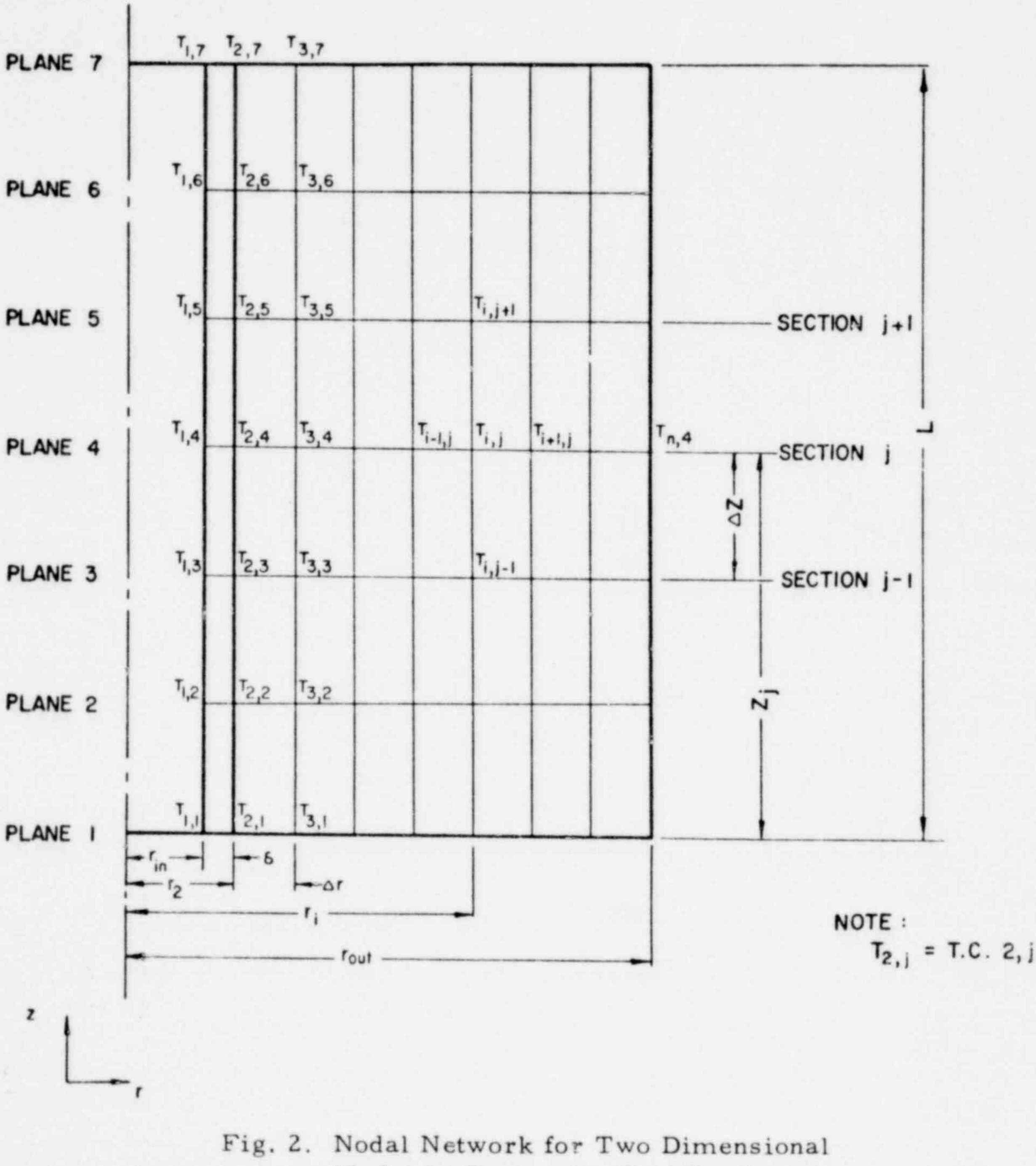

Fig. 2. Nodal Network for Two Dimensional Model in Composite Test Section

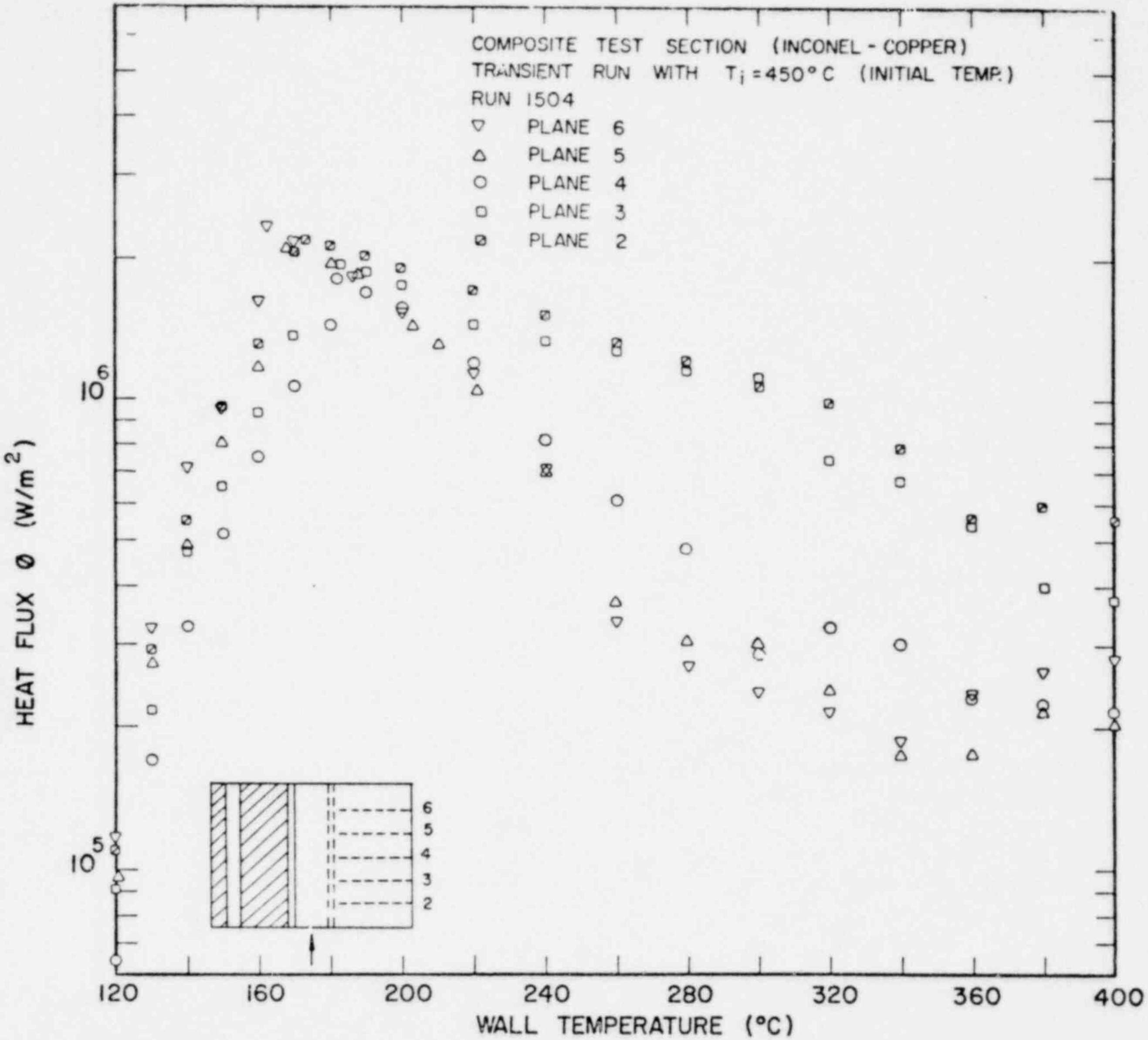

Fig. 3. Boiling Curves of Distilled Water, 1500 Run Series for $G = 136\ kg/m^2s$ and $T_{sub} = 13.9°C$, Using 2-D Model

1372 139

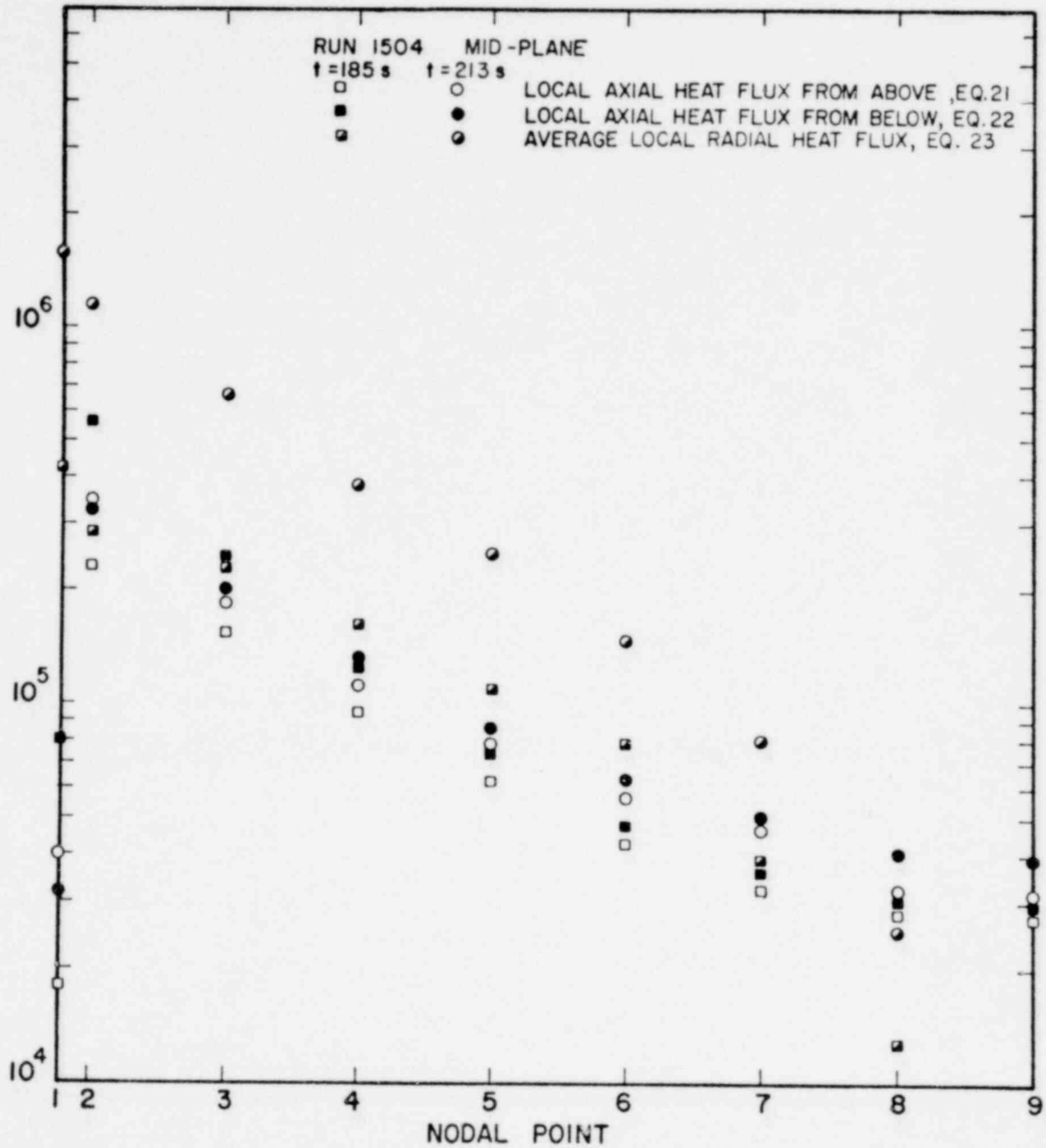

Fig. 4. Local Axial Heat Flux Distribution at Mid-Section for Inconel-Copper Composite Test Section for $G = 136\ kg/m^2s$ and $\Delta T_{sub} = 13.9°C$ (Part I)

1372 140

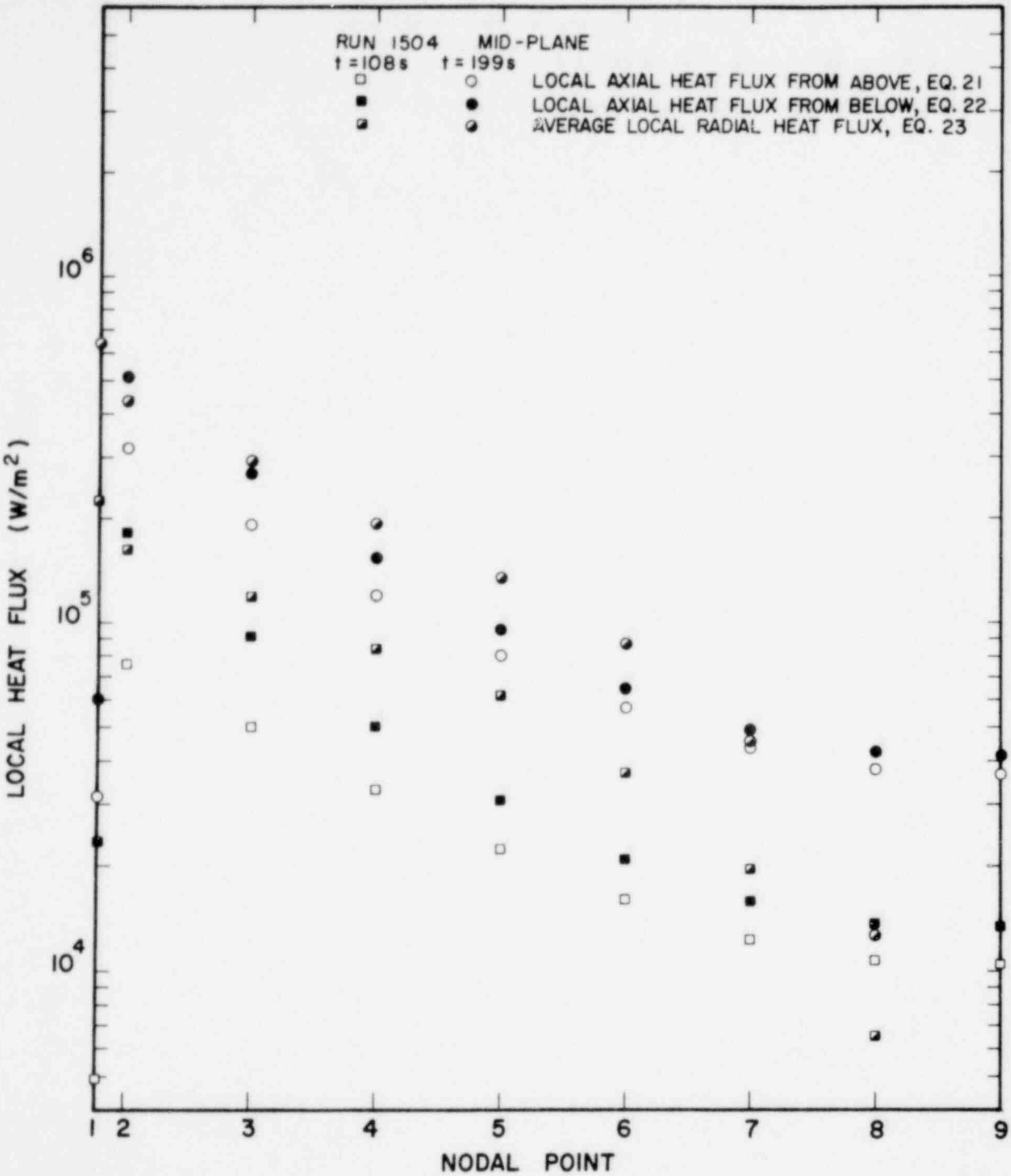

Fig. 5. Local Axial Heat Flux Distribution at Mid-Section for Inconel-Copper Composite Test Section for $G = 136\ kg/m^2s$ and $\Delta T_{sub} = 13.9°C$ (Part II)

1372 141

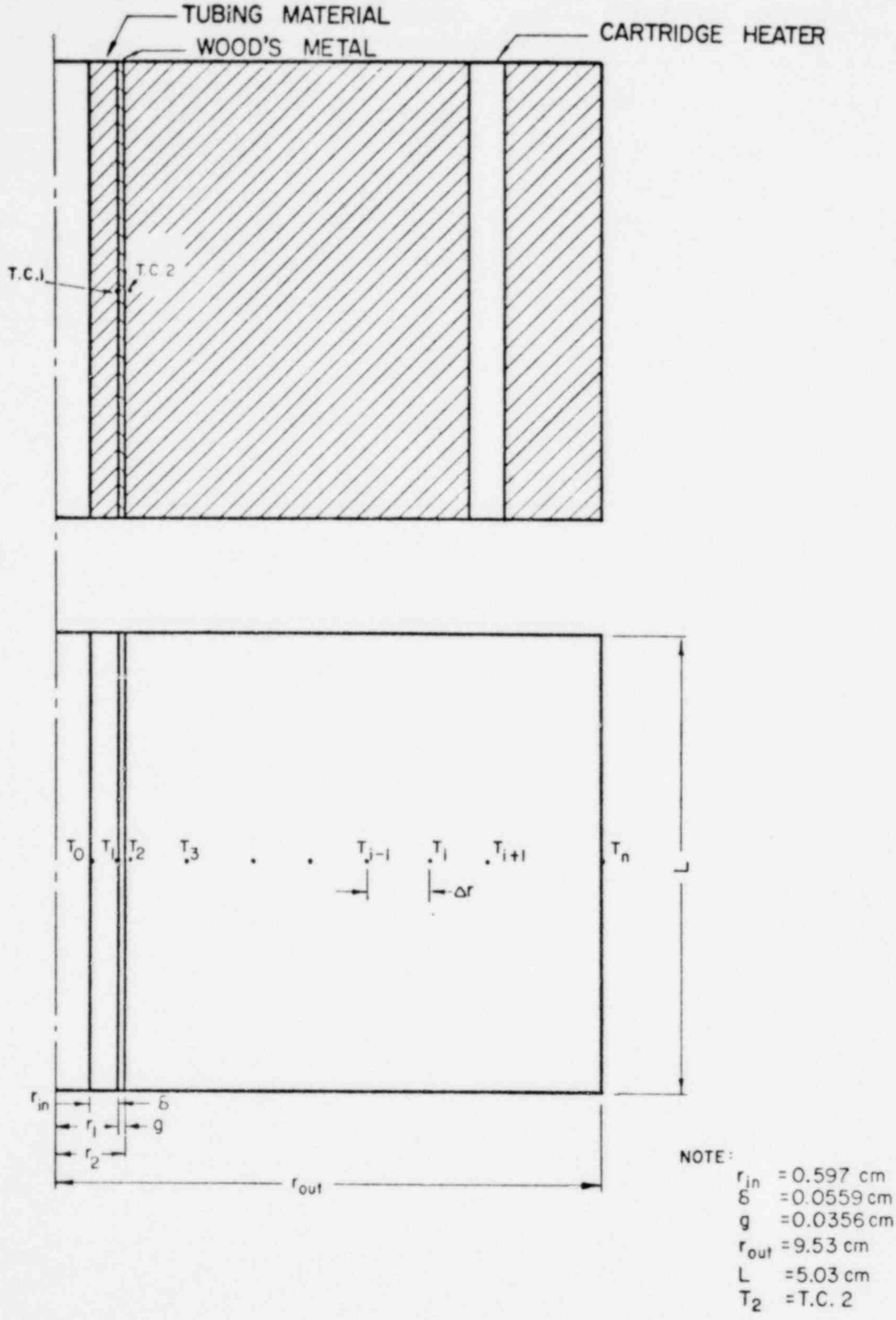

Fig. 6. Zircaloy-Copper Composite Test Section and Its Model Point Distribution

1372 142

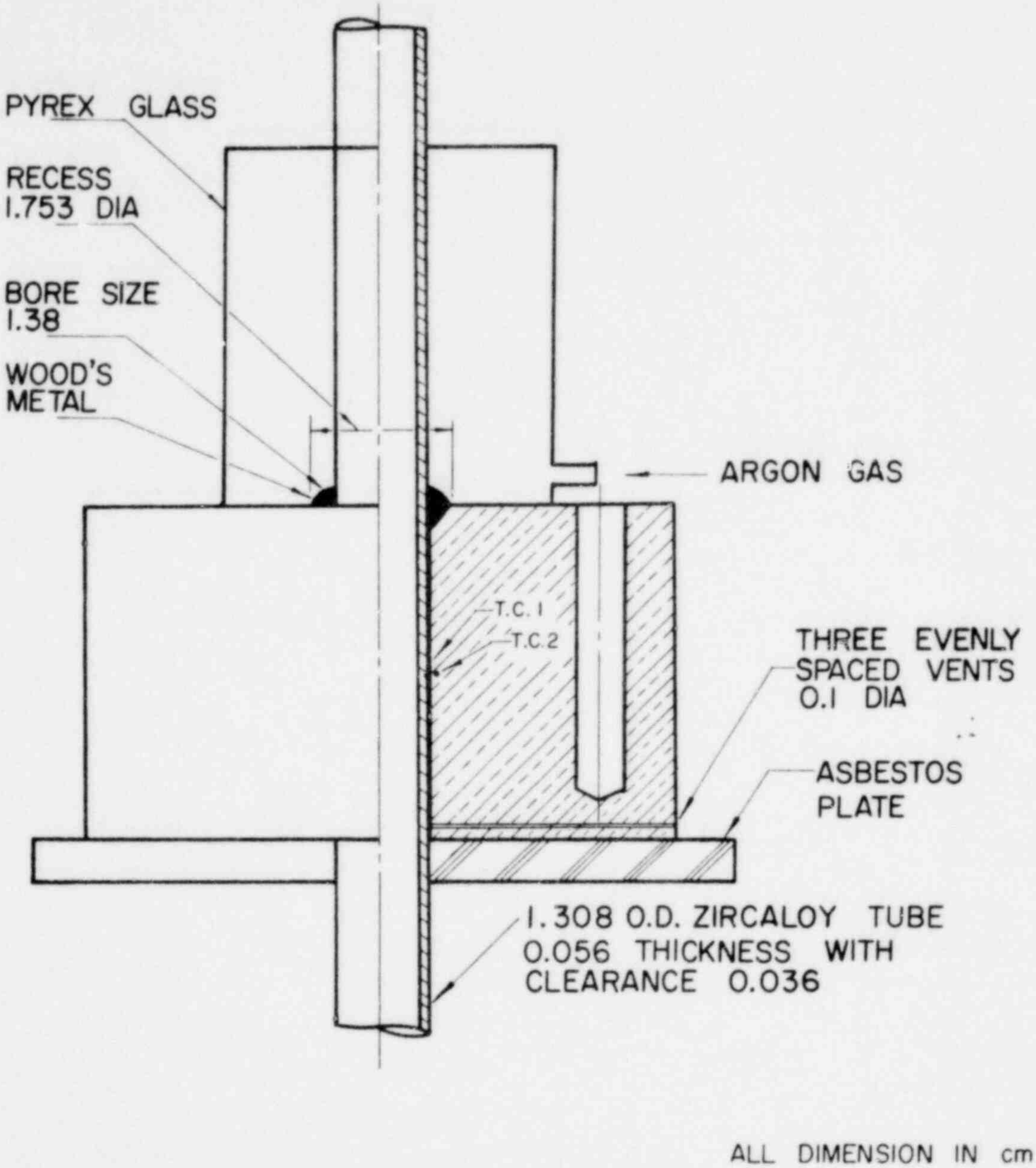

Fig. 7. Detailed Zircaloy-Copper Composite Test Section

1372 143

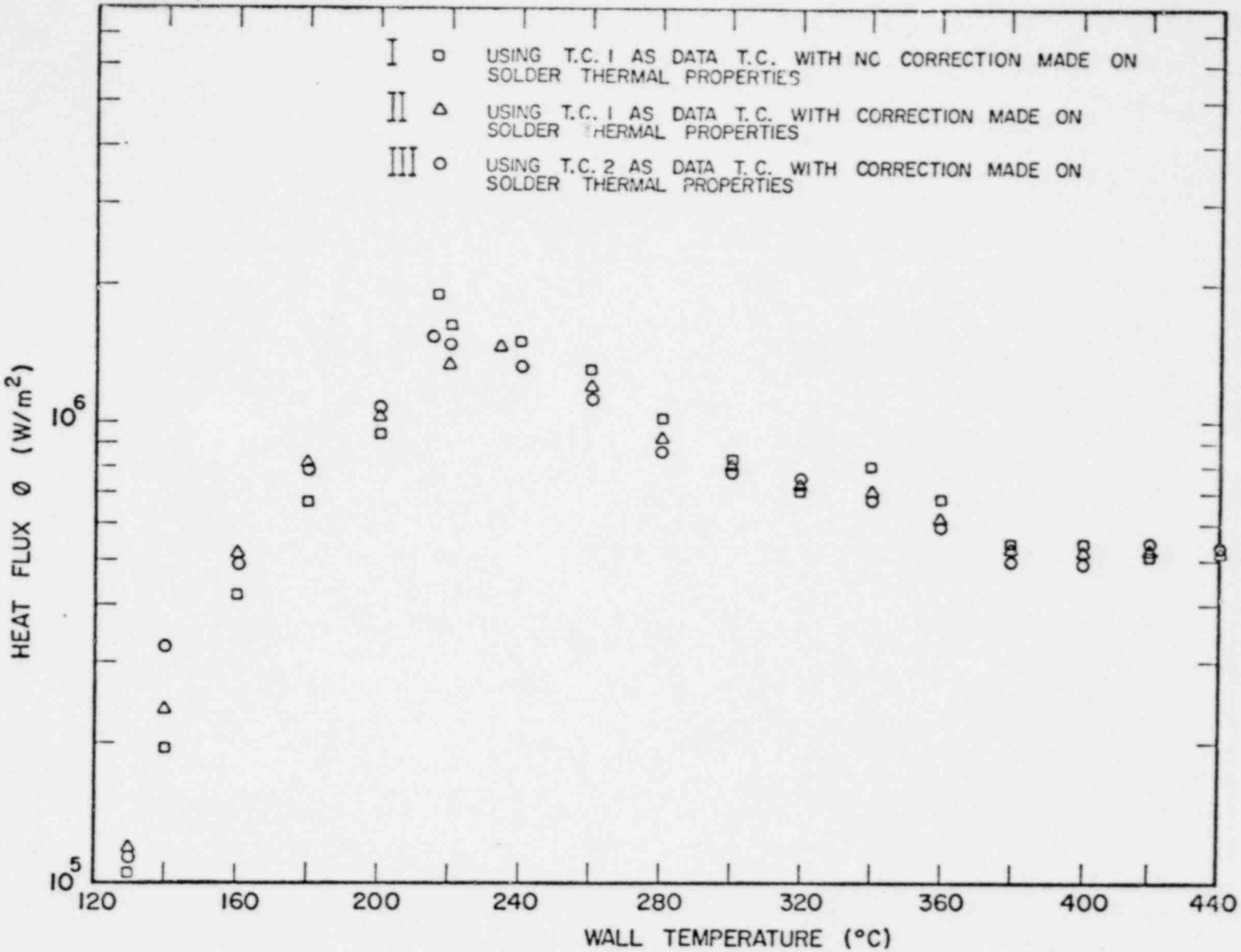

Fig. 8. Boiling Curve for Distilled Water, 1700 Run Series for G = 203 kg/m^2s and ΔT_{sub} = 13.9°C

1372 144

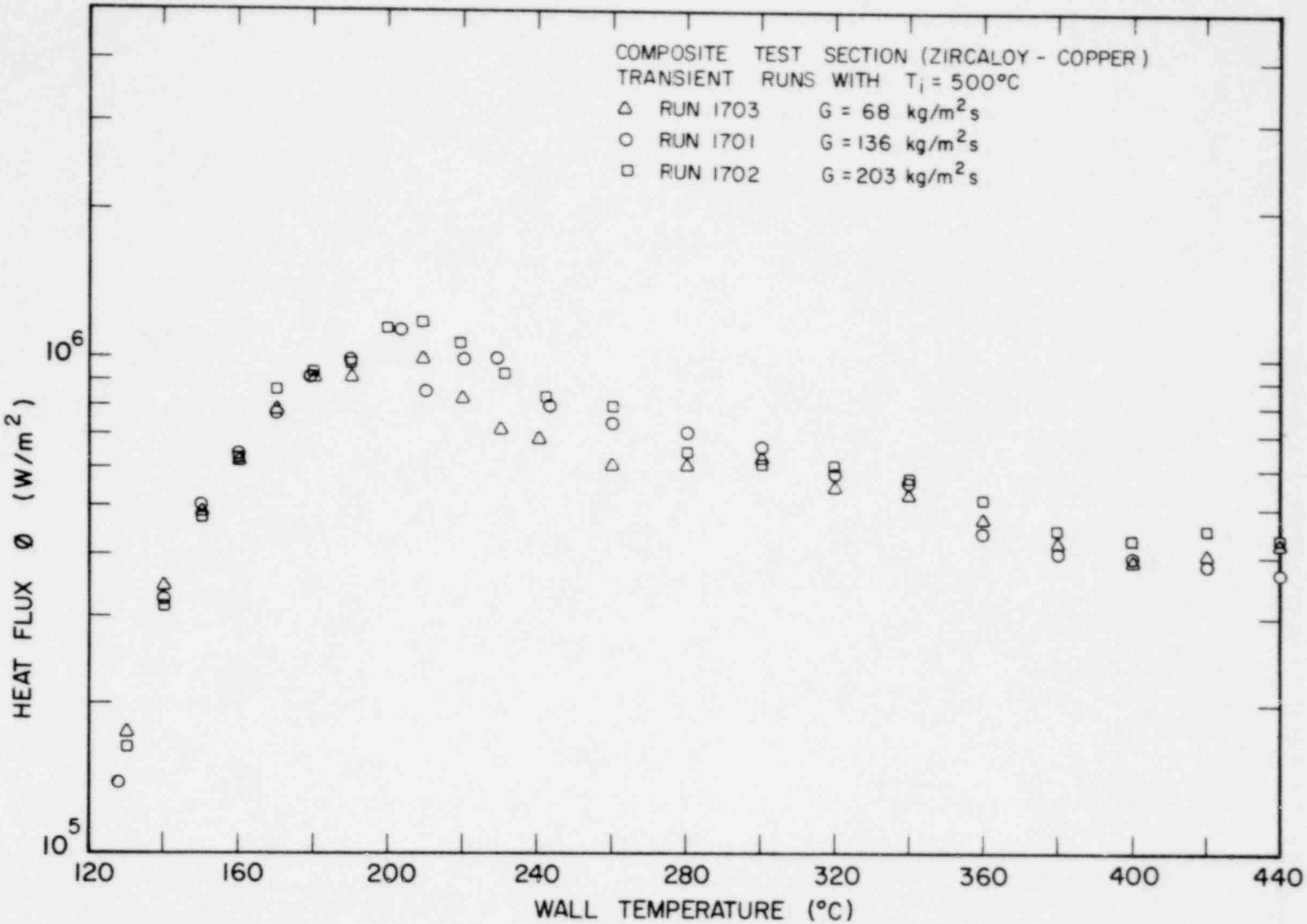

Fig. 9. Boiling Curves for Distilled Water, 1700 Run Series for ΔT_{sub} = 13.9°C

1372 145

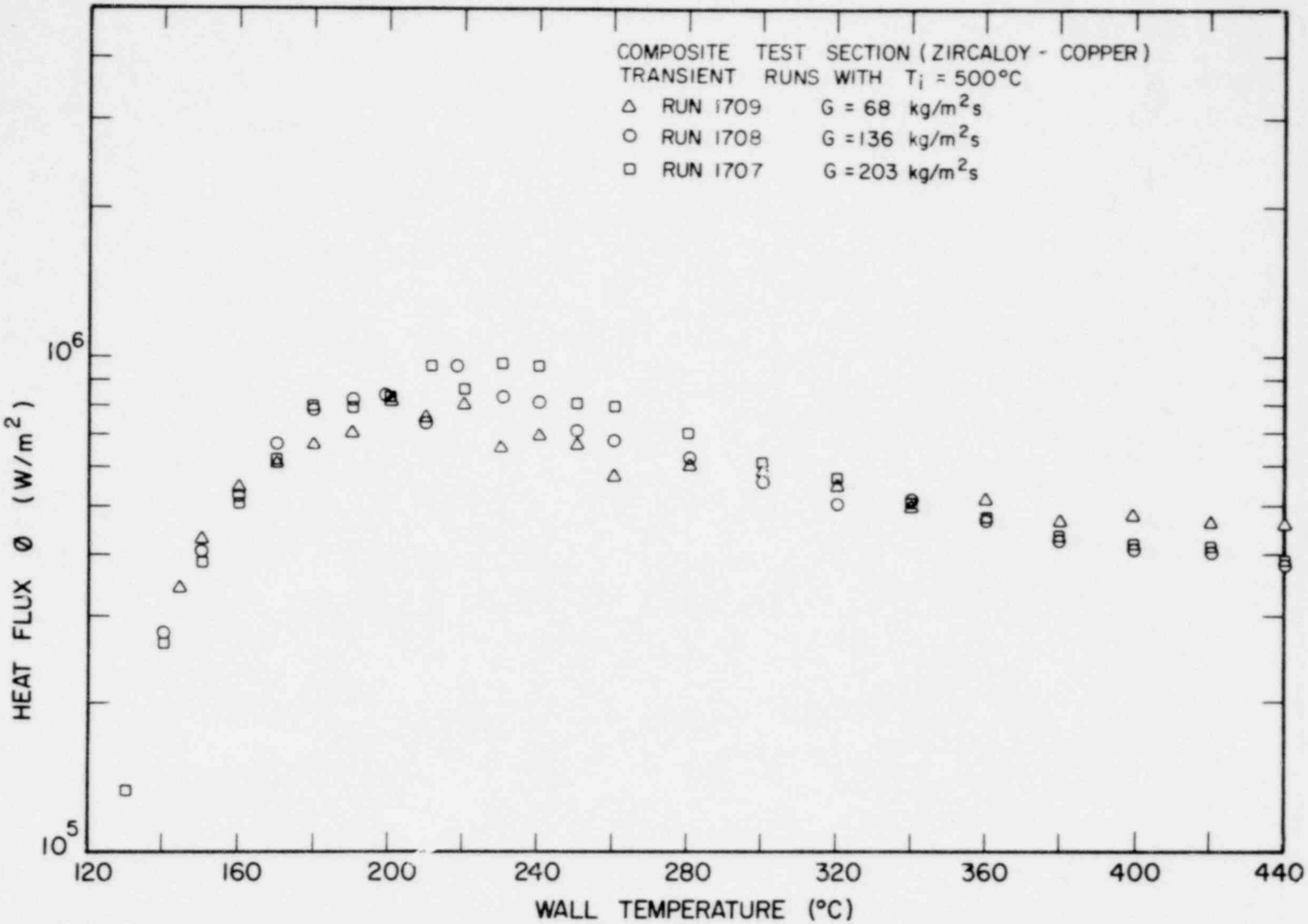

Fig. 10. Boiling Curves for Distilled Water, 1700 Run Series for ΔT_{sub} = 0°C

1372 146

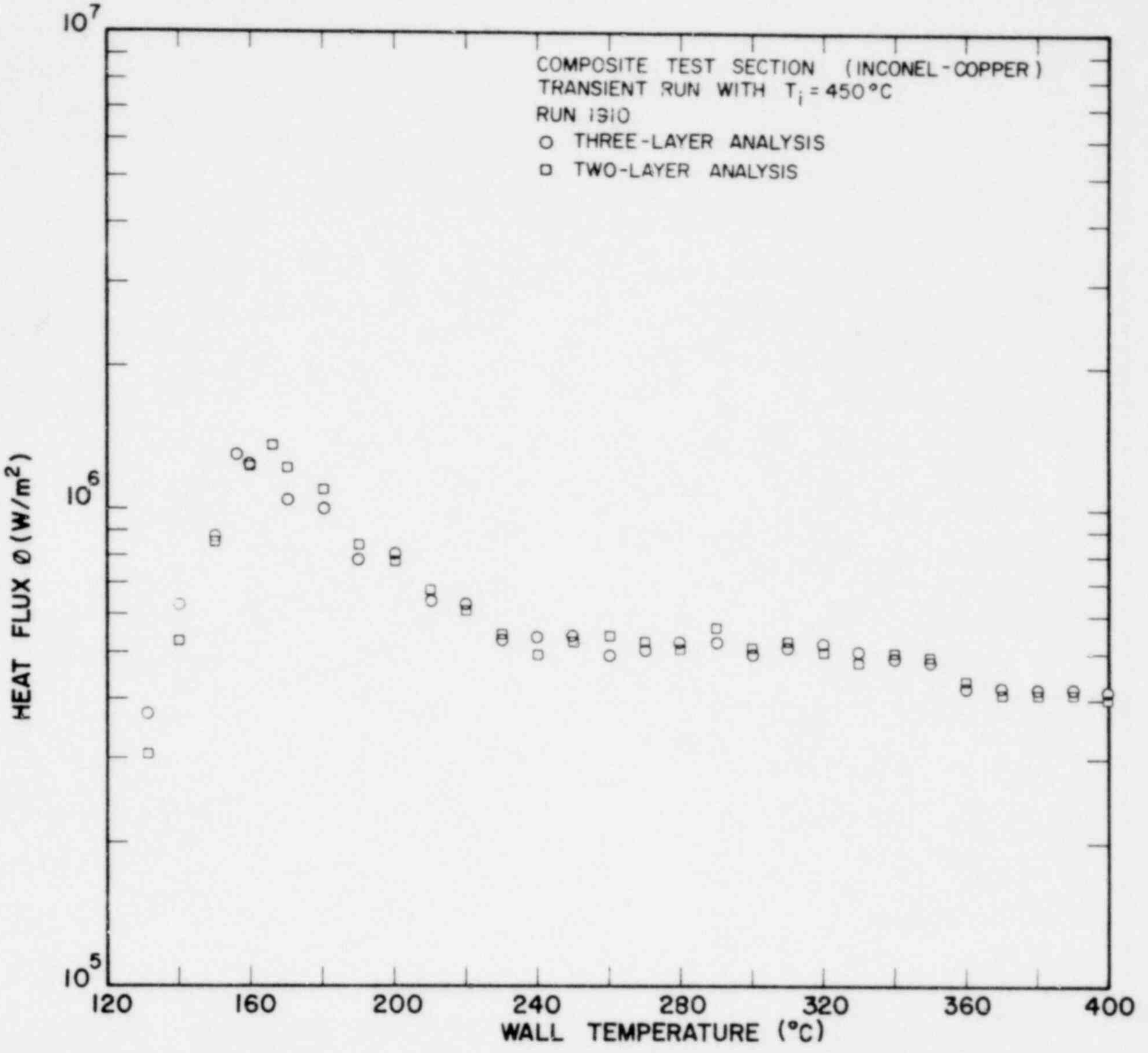

Fig. 11. Comparison of Boiling Curves for Three-layer and Two-layer Analyses, 1900 Run Series for $G = 136\ kg/m^2s$ and $\Delta T_{sub} = 13.9°C$

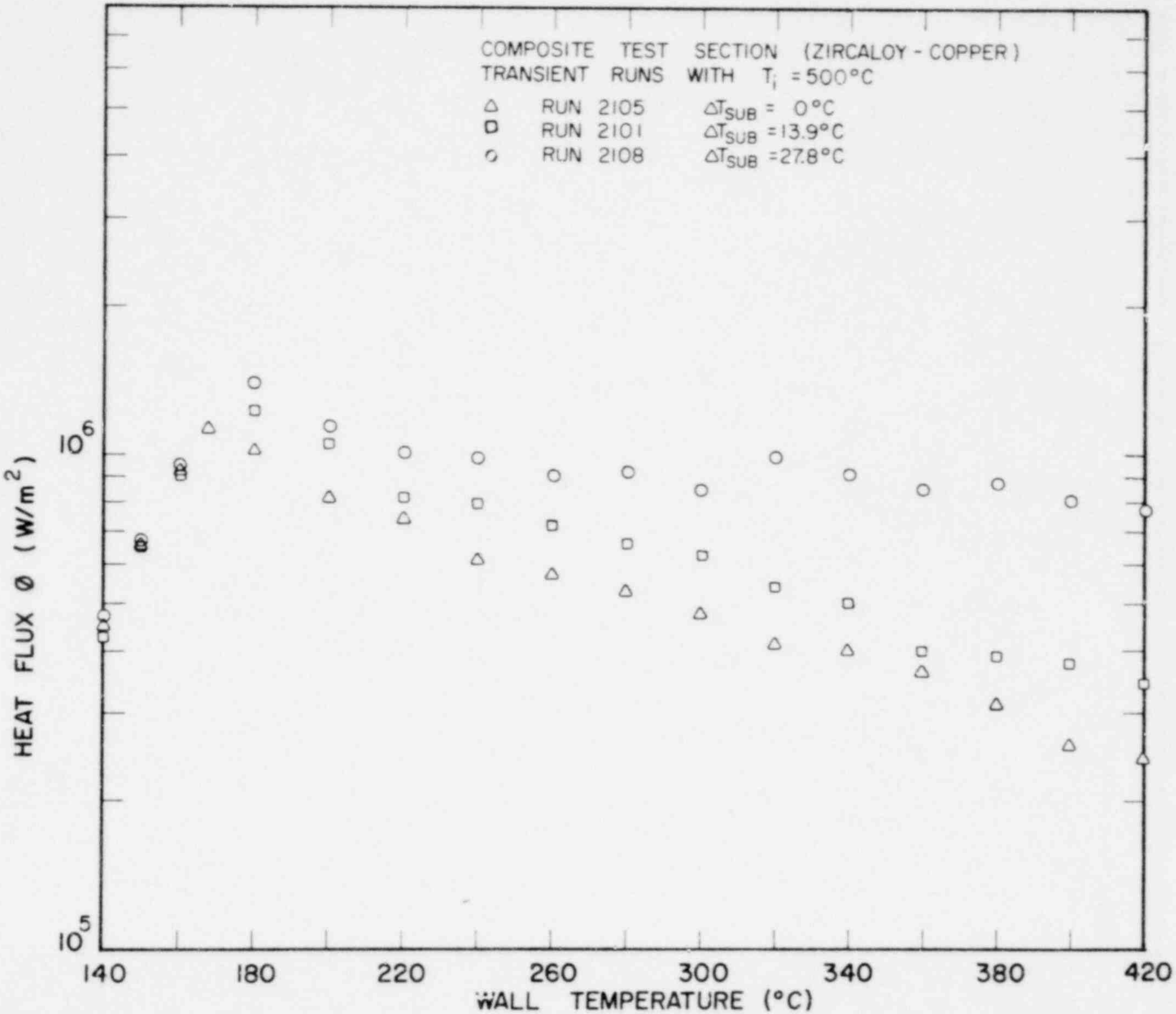

Fig. 12. Boiling Curves of Distilled Water, 2100 Run Series for G = 136 kg/m^2s, Using 1-D Model

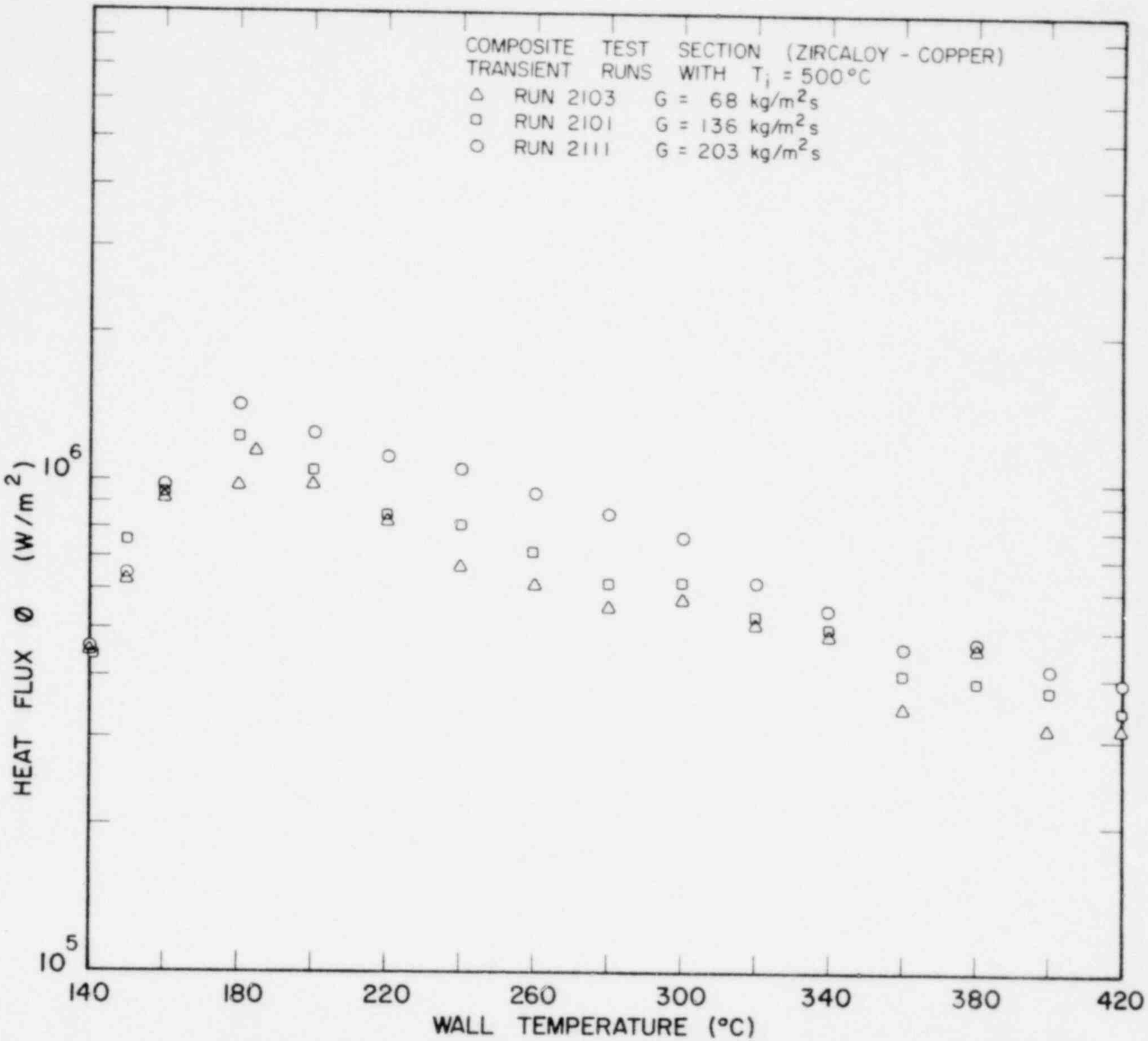

Fig. 13. Boiling Curves of Distilled Water, 2100 Run Series for ΔT_{sub} = 13.9°C, Using 1-D Model

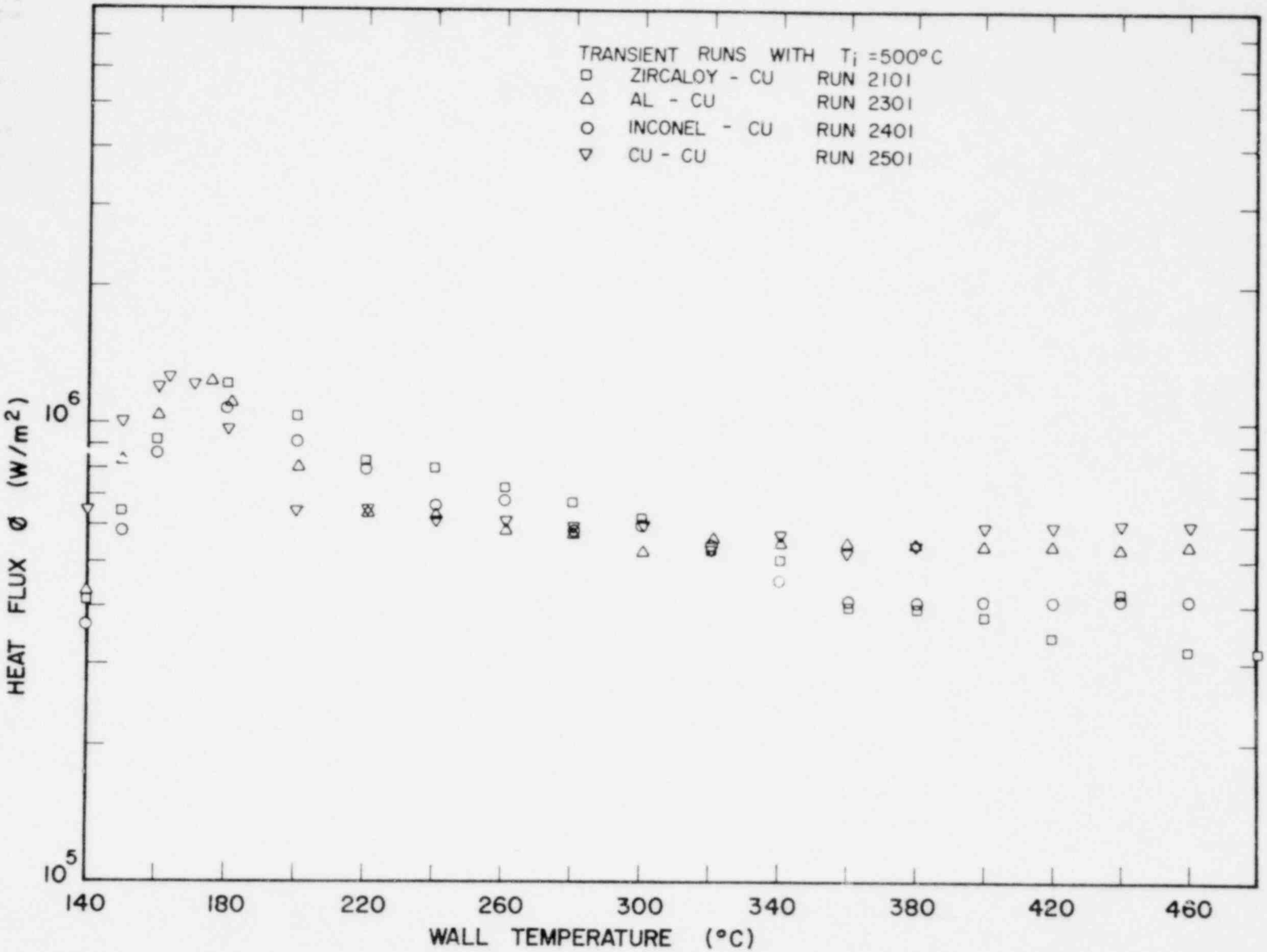

Fig. 14. Comparison of Boiling Curves for Various Heated Surfaces at G = 136 kg/m^{2}s and ΔT_{sub} = 13.9°C, Using 1-D Model

1372 150

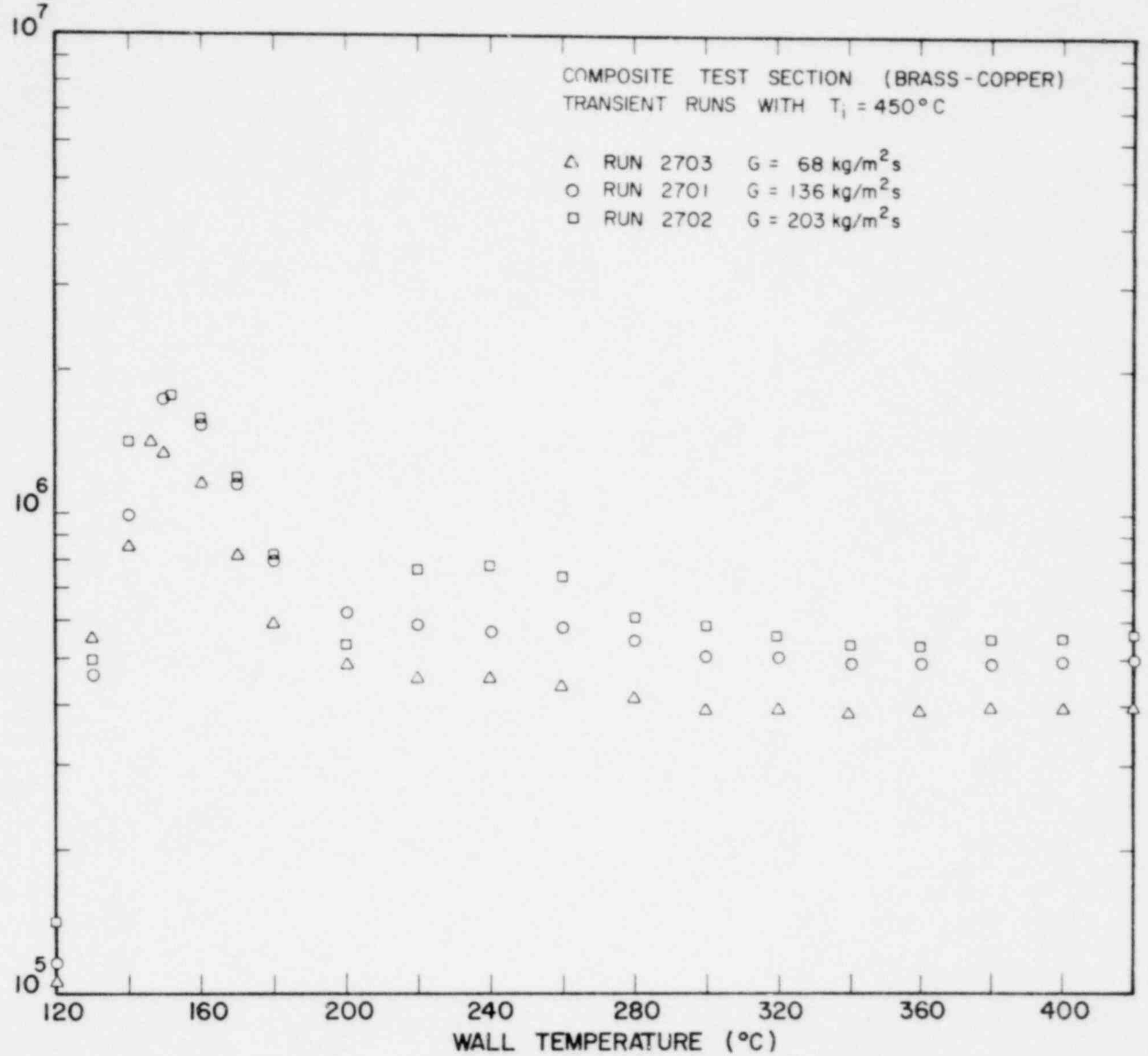

Fig. 15. Boiling Curves of Distilled Water, 2700 Run Series for ΔT_{sub} = 13.9°C

1372 151

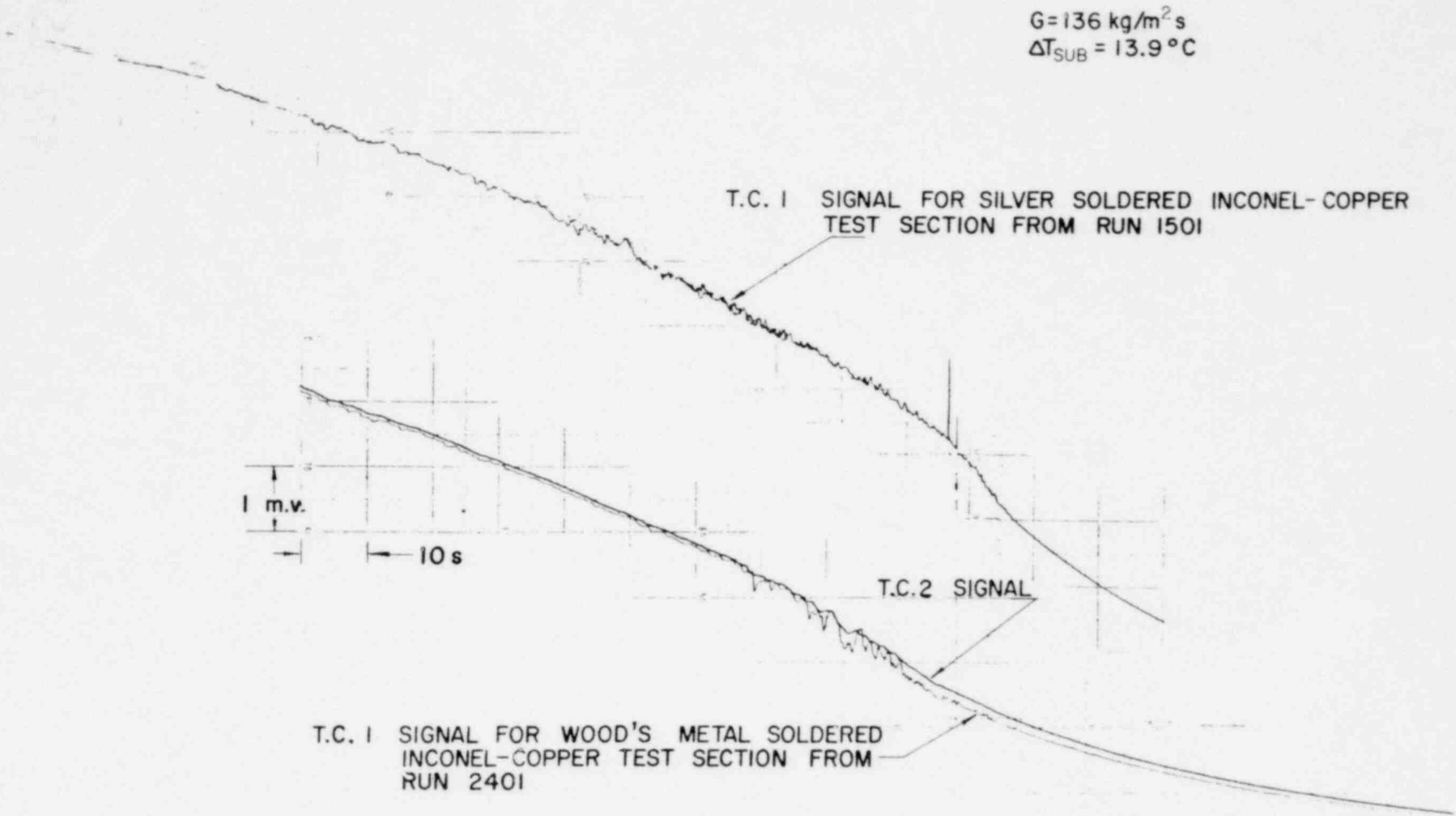

Fig. 16. Thermocouple Recordings from Silver Soldered Inconel-Copper Test Section and Wood's Metal Soldered Inconel-Copper Test Section

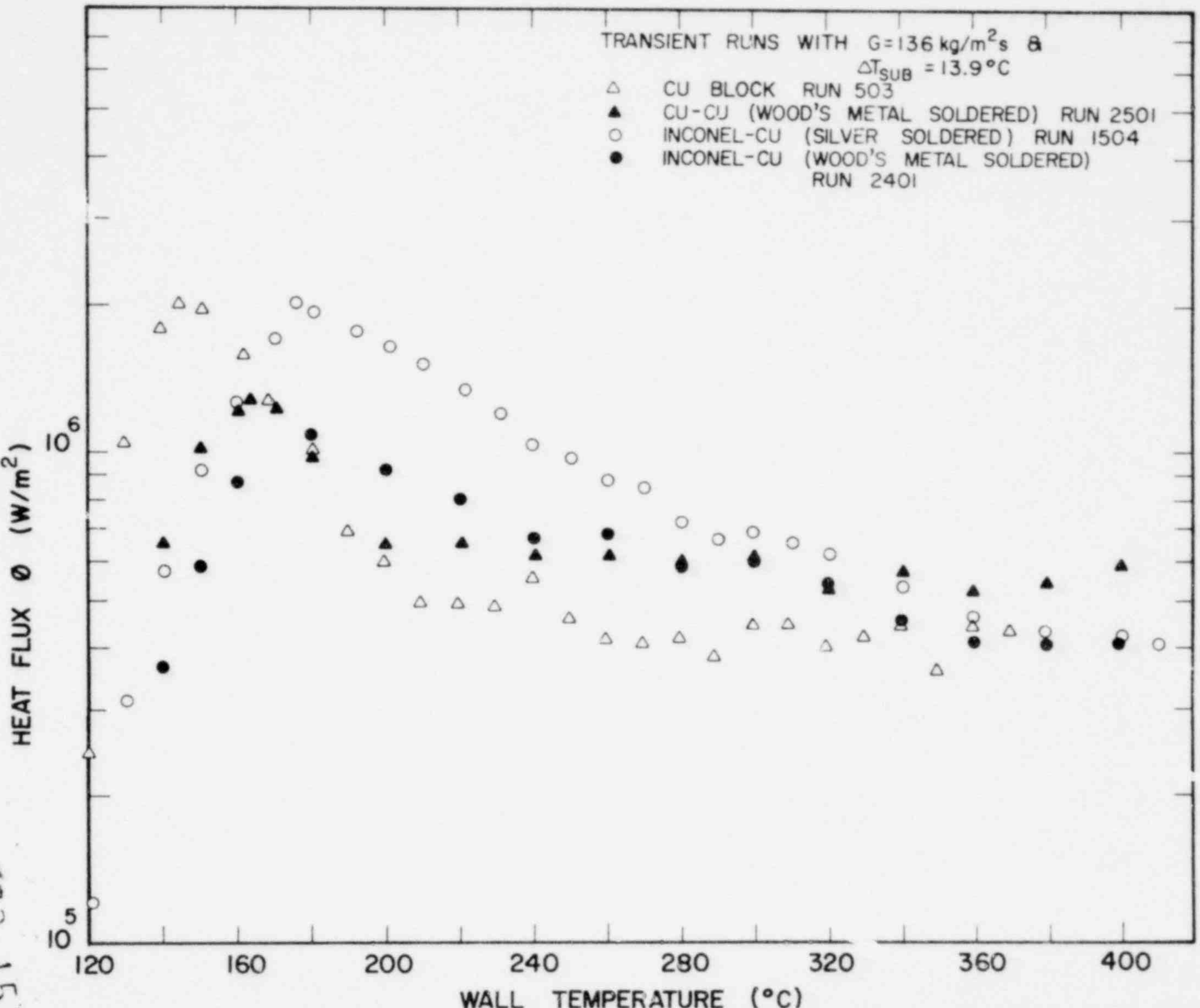

1372 153

Fig. 17. Comparison of Boiling Curves from Wood's Metal Soldered Composite Test Sections with Other Data

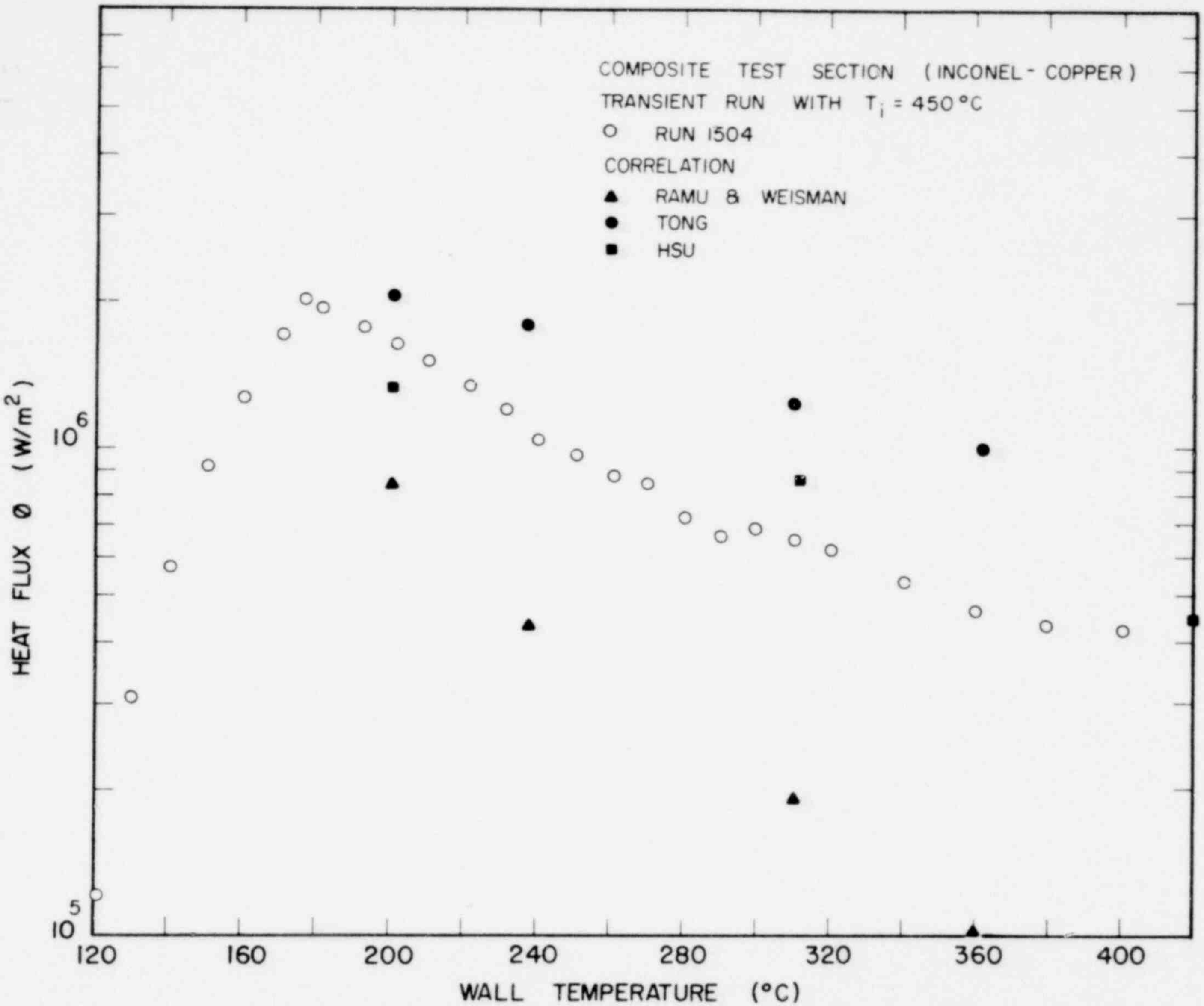

Fig. 18. Comparison of Data for 1500 Run Se... s with $G = 136$ kg/m^{2}s and $\Delta T_{sub} = 13.9$°C

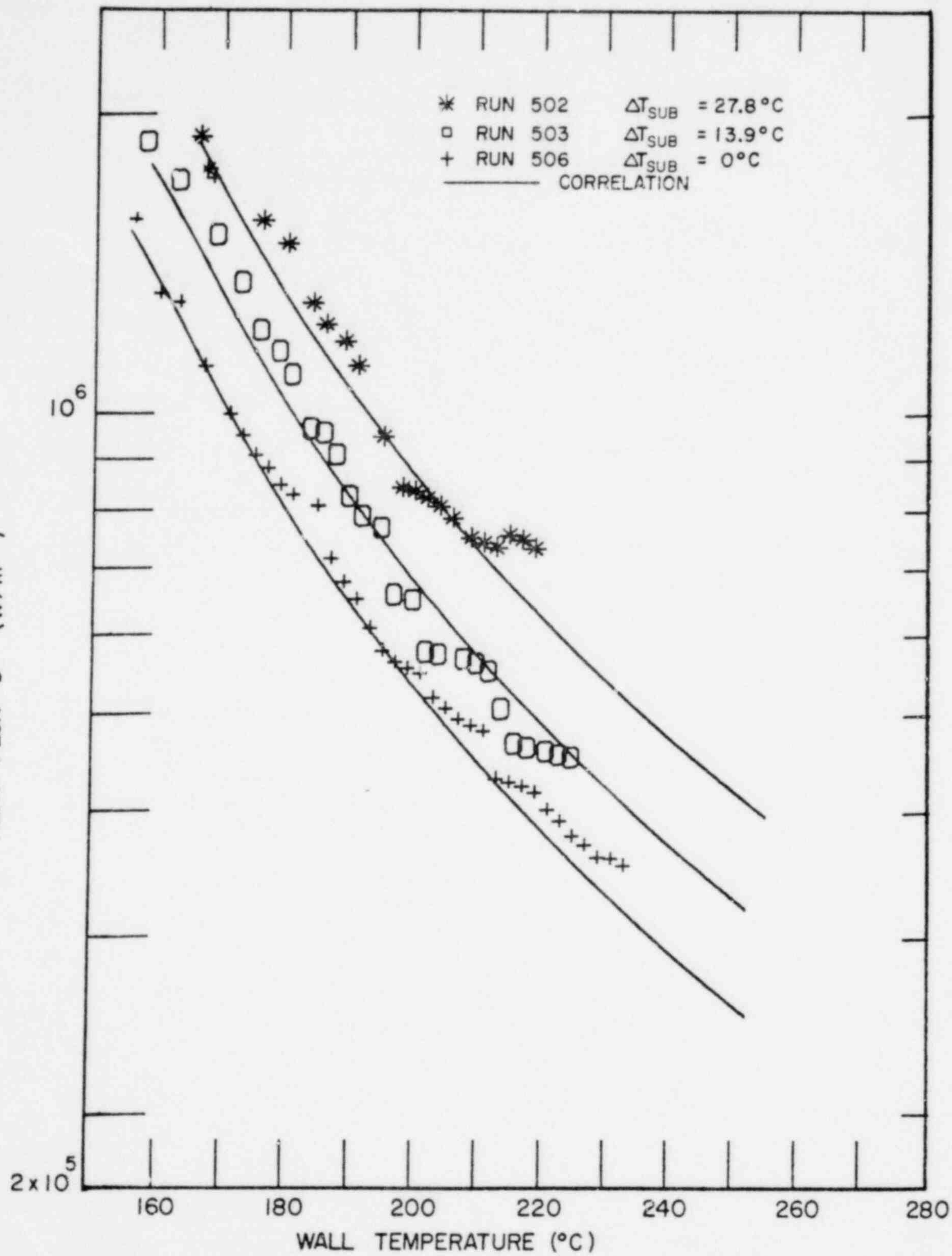

Fig. 19. Comparison of Copper Correlation with Transition Boiling Data for G = 136 kg/m^{2}s

. 1372 155

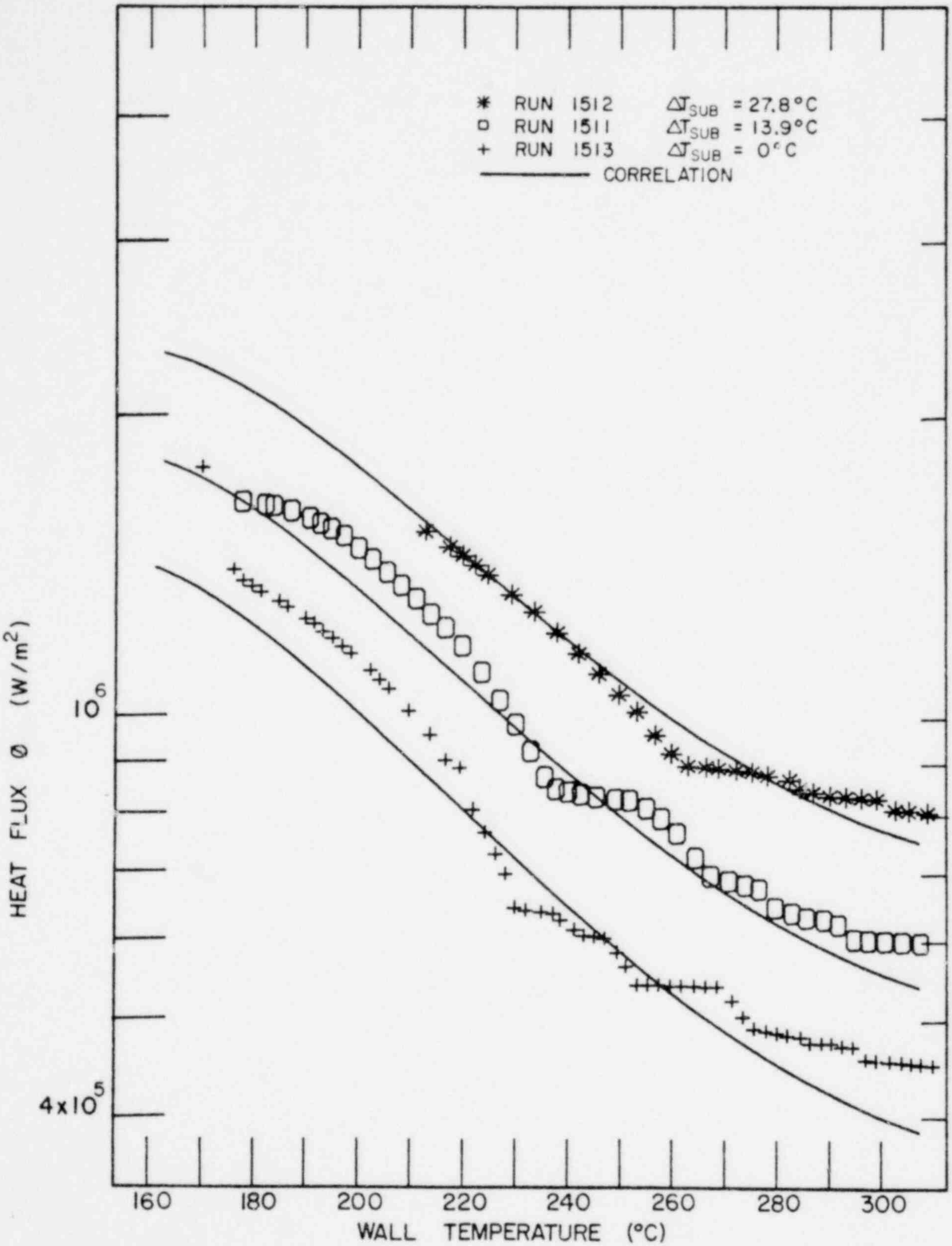

Fig. 20. Comparison of Inconel Correlation with Transition Boiling Data for $G = 68\ kg/m^2s$

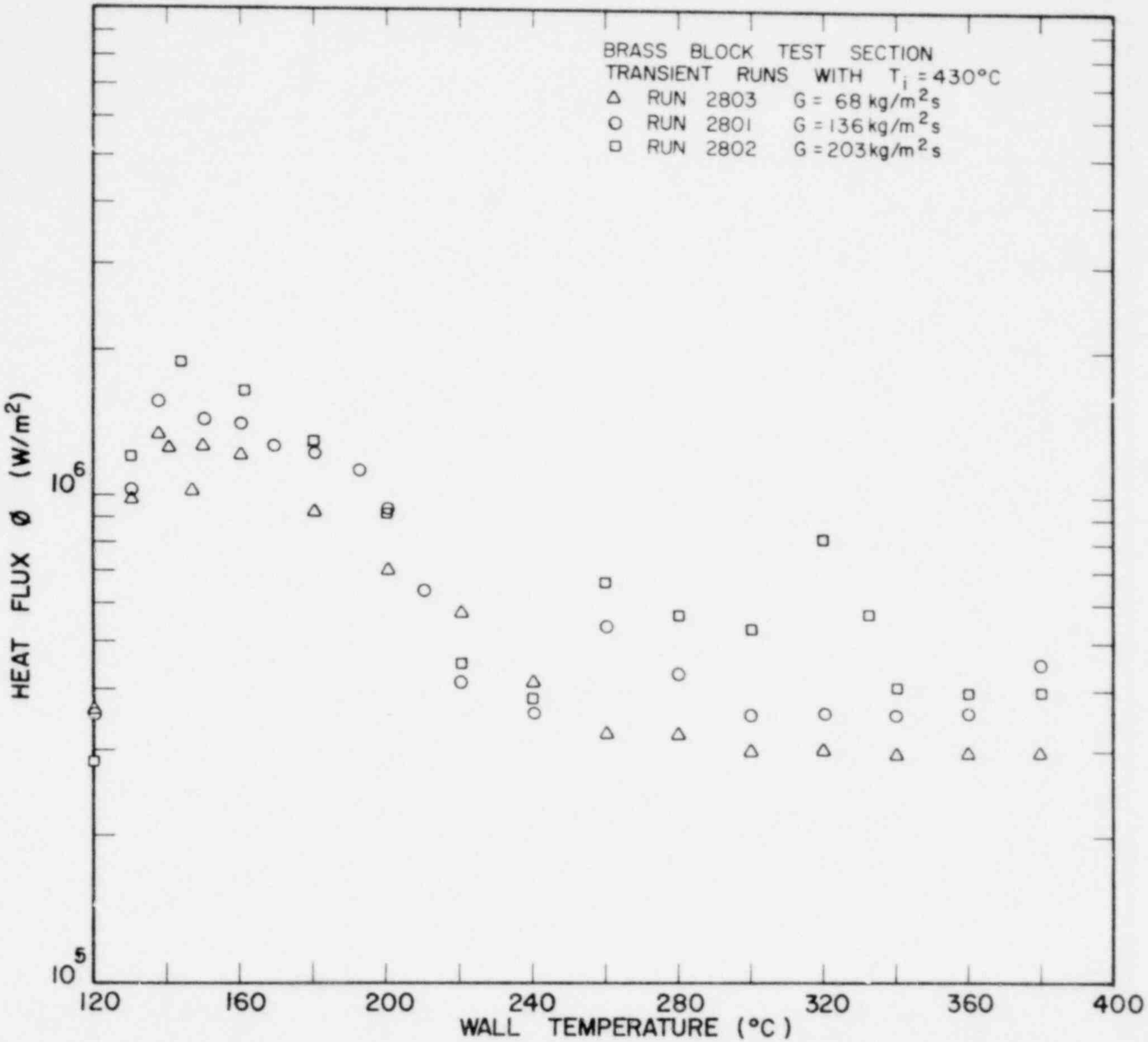

Fig. 21. Boiling Curves of Distilled Water, 2800 Run Series for ΔT_{sub} = 13.9°C

1372 157

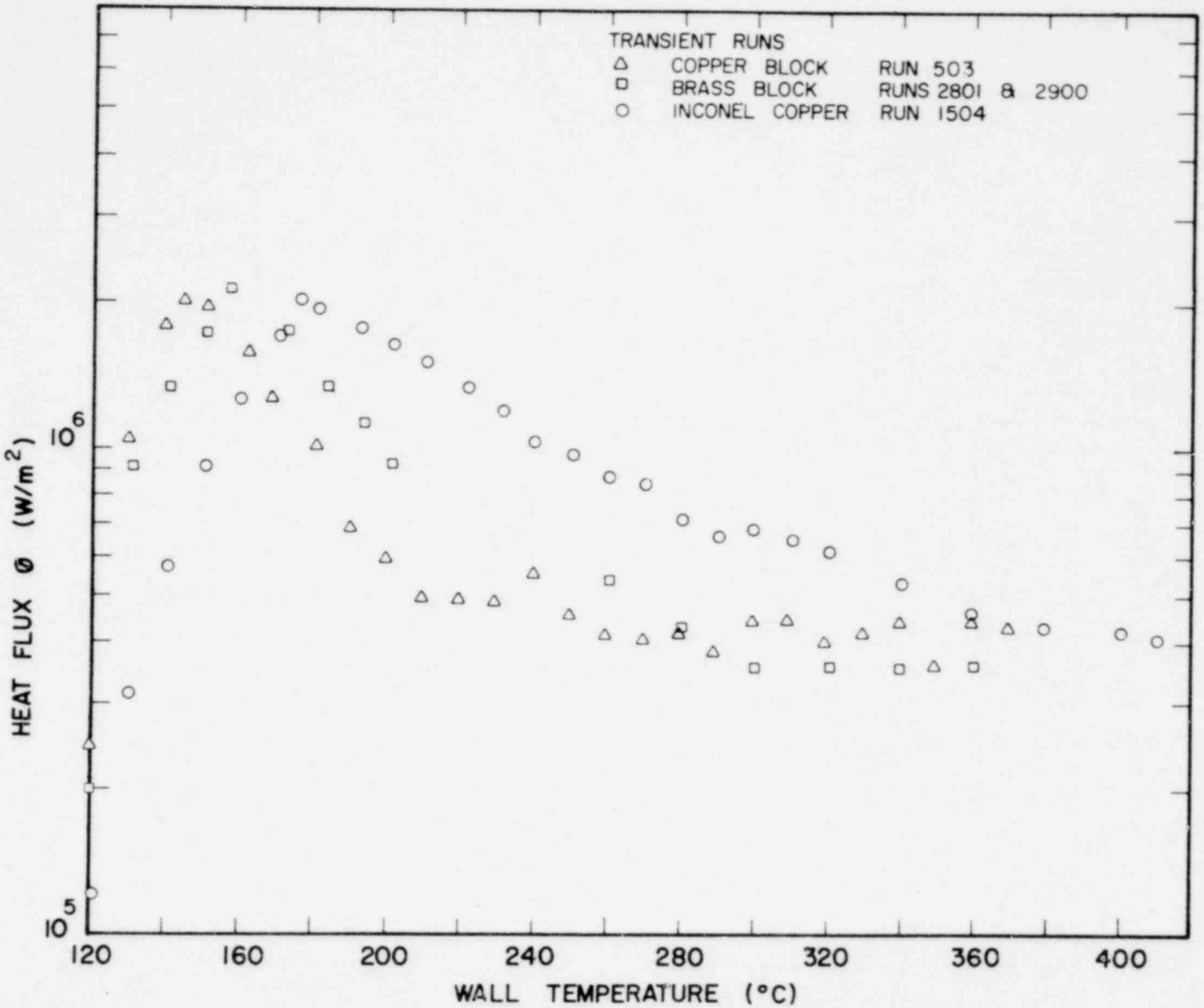

Fig. 22. Comparison of Boiling Curves for Copper, Brass and Inconel Heated Surfaces at $G = 136\ kg/m^2s$ and $\Delta T_{sub} = 13.9°C$

1372 158

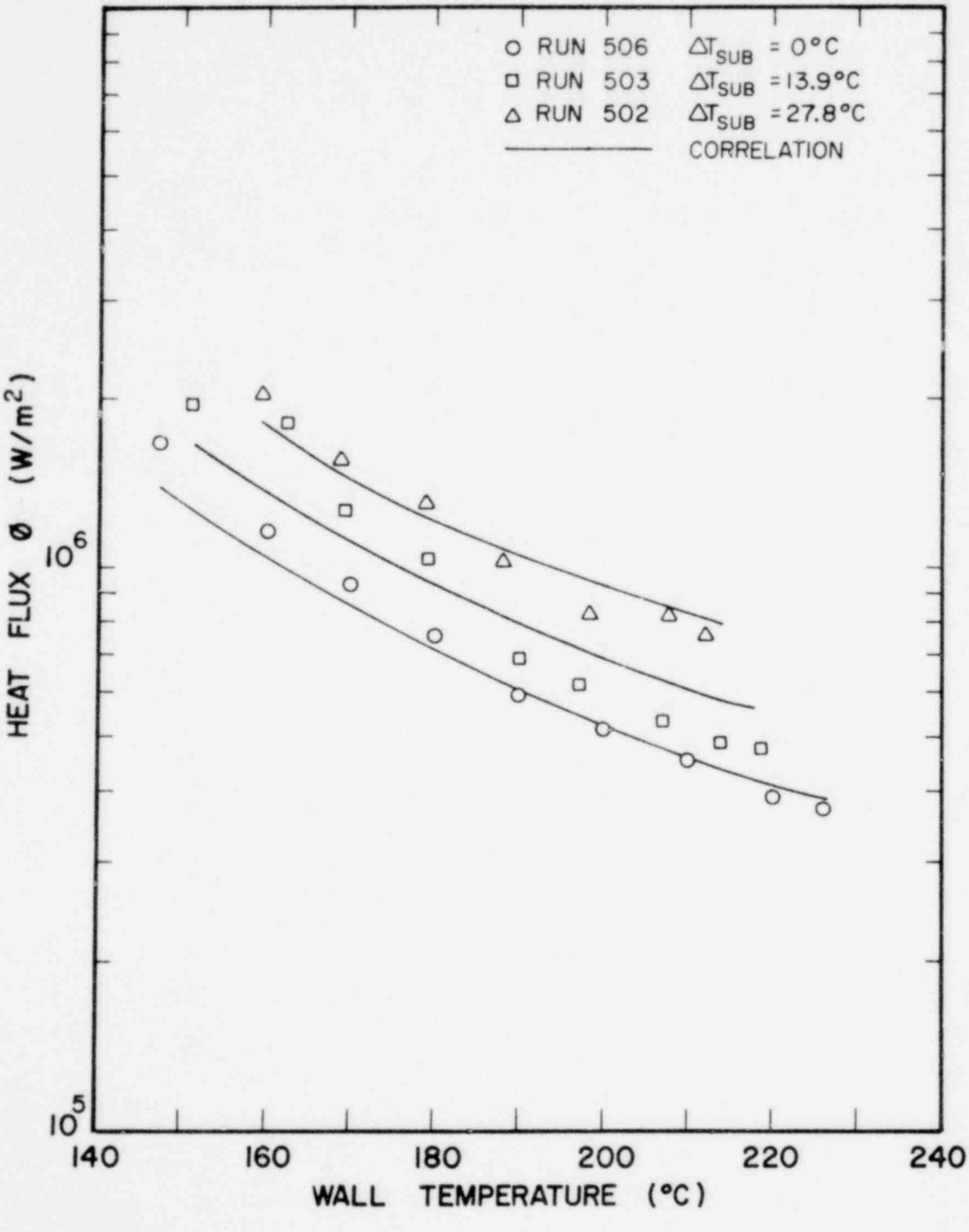

Fig. 23. Comparison of General Empirical Correlation with Copper Data for G = 136 kg/m^{2}s

1372 159

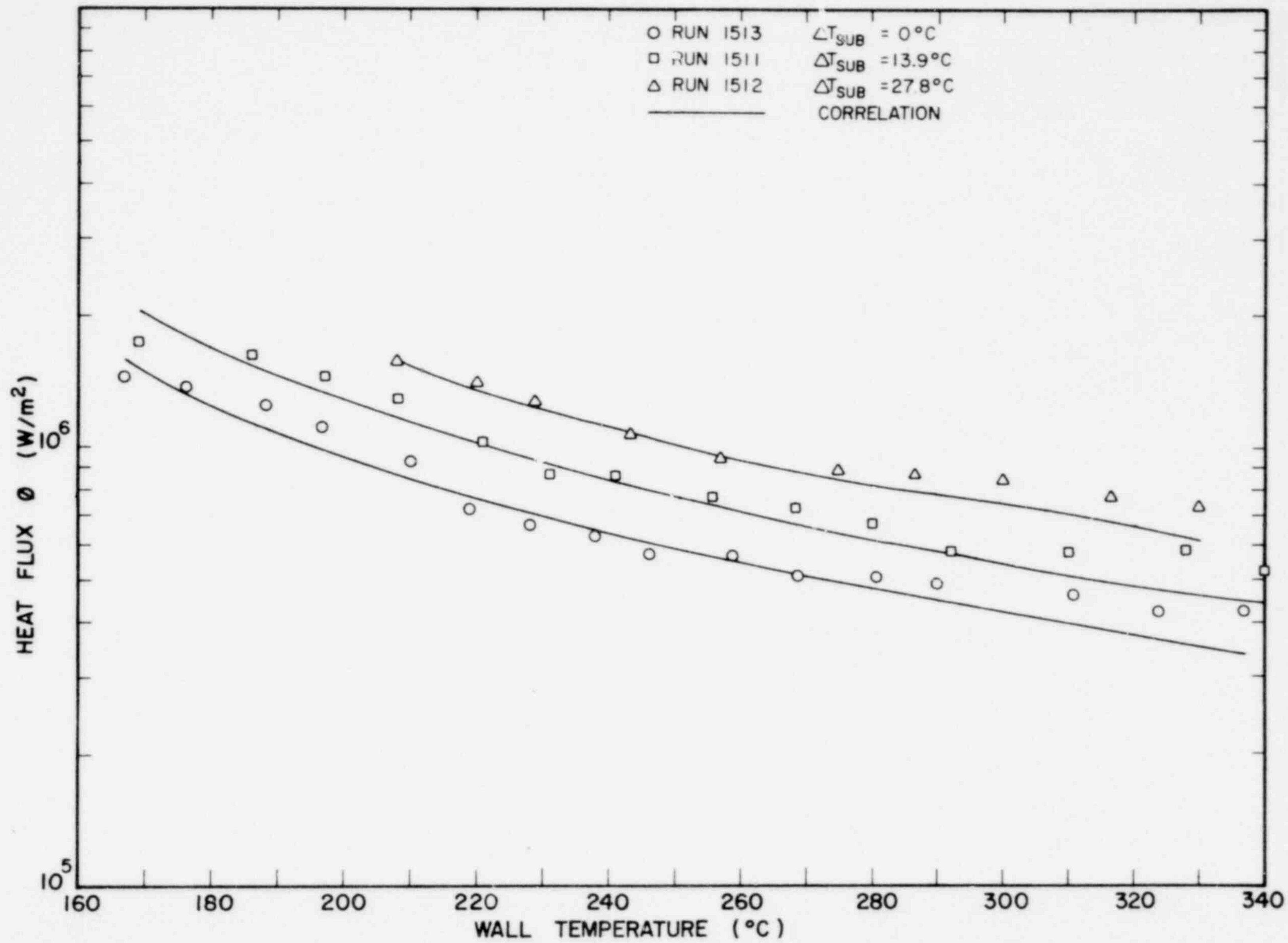

Fig. 24. Comparison of General Empirical Correlation with Inconel Data for G = 68 kg/m²s

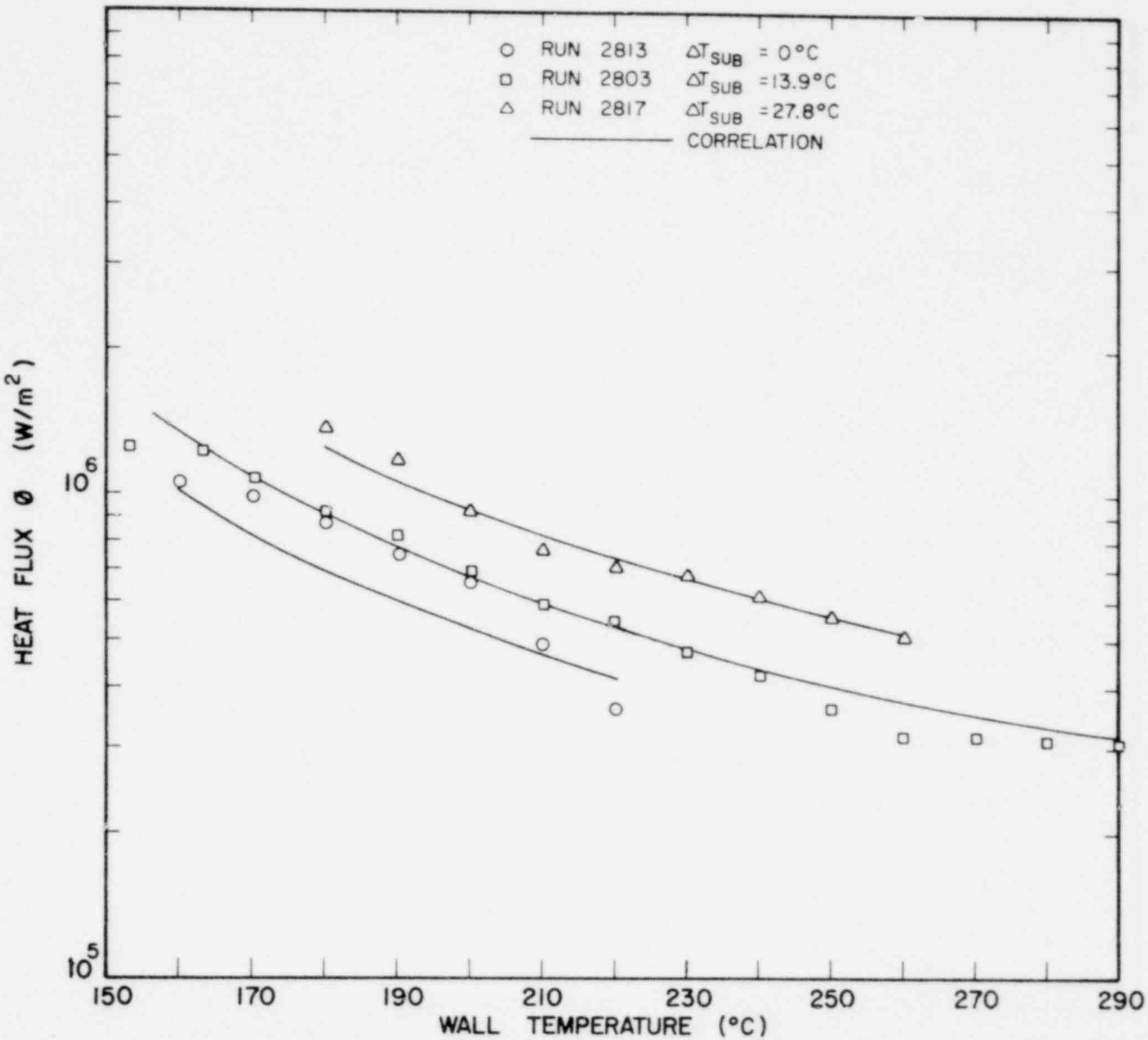

Fig. 25. Comparison of General Empirical Correlation with Brass Data for G = 68 kg/m^{2}s

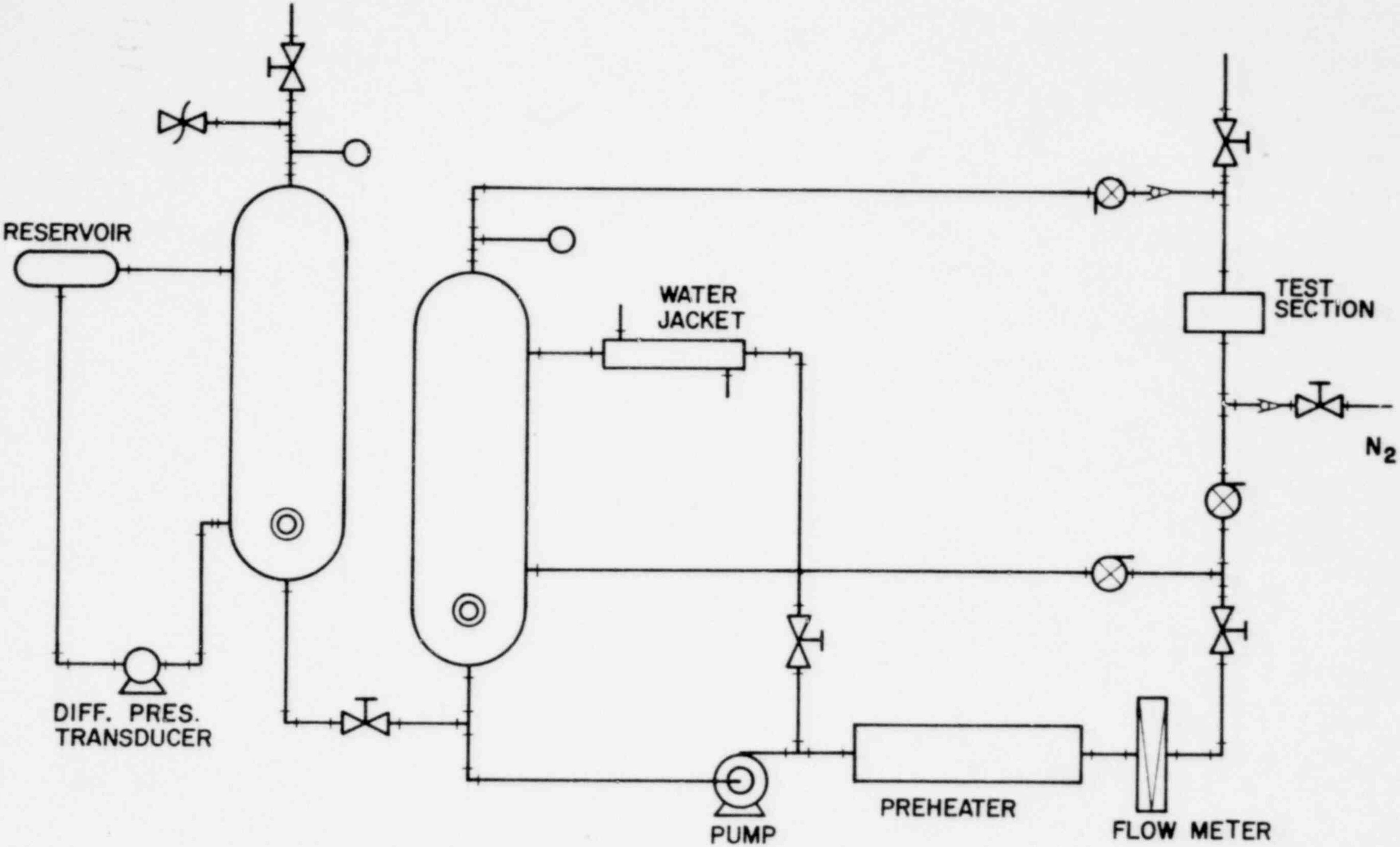

Fig. 26. Preliminary Design for Pressurized Loop

APPENDIX I

Steady State Flow Boiling Curve Measurement Via Temperature Controllers

1372 163

STEADY STATE FLOW BOILING CURVE MEASUREMENTS VIA TEMPERATURE CONTROLLERS

W. W. L. Ng
Department of National Defence

S. C. Cheng
University of Ottawa
Ottawa, Canada

Introduction

The feasibility of using temperature controllers to measure flow boiling data under steady state condition has been demonstrated previously [1,2,3]. Due to insufficient power rating of heaters and process controlling problems, only boiling data at lower heat flux regions were obtainable. In this study, the technique has been improved, thus allowing the construction of an entire boiling curve.

Apparatus and Experimental Method

The test section as shown in Fig. 1 consists of a 5.08 cm long cylindrical copper block with 9.53 cm outside diameter and a center bore of 1.296 cm allowing for the insertion of an Inconel tube. The Inconel tube with OD = 1.27 cm and thickness = 0.038 cm is inserted into the copper block, a gap of 0.013 cm between them is provided for before silver soldering. The Inconel tube is sticking out from both ends of test section for piping connections. This arrangement is designed to damp temperature fluctuation during experiments due to high thermal inertia of copper. In addition, for transient boiling experiments (quenching) [1,2,3], the high heat capacity of copper will sustain a long cooldown period, thus permitting frequent and accurate temperature measurements.

Twenty-four cartridge heaters with 250 W each are spaced around the test section in two arrays as shown in Fig. 1. A total of six thermocouples are embedded, five of them located at the interface of the tube and silver solder. The test section is insulated by thick ceramic fiber insulation.

Two types of temperature controllers are used to control the power input to heaters, i.e. an ON-OFF temperature controller (Model R7353, Honeywell) and a proportional temperature controller (Model R7355, Honeywell). The proportional controller is regulated by a Silicon Controlled Rectifier driver stage (Model LZF1, SCR Driver, Halmar). The S.C.R. driver acts as a current valve to regulate the current input to heaters in proportion to the deviation between the set-point temperature and the controlling temperature (T.C.C 2 of Fig. 1).

Various attempts have been made to control the power input to heaters by the two controllers. The arrangement with the inner array of heaters controlled by the proportional controller and the outer array of heaters by the ON-OFF controller proves to be most satisfactory. T.C.C 2 is used as a common temperature sensor for both controllers.

Subcooled distilled water at atmospheric conditions is introduced from the bottom of the test section during experiments. The temperature of the test section (T.C.C 1, Fig. 1) is initially set well into the film boiling régime and is maintained at that level by the controllers during the run. The experiment is then repeated at lower heated surface temperatures until a complete boiling curve is obtained. Detailed experimental apparatus and procedures may be found in [1,3].

Results and Discussion

A typical boiling curve for a mass flux of 136 kg/m²s and subcooling of 13.6°C is shown in Fig. 2. Wall temperatures in the boiling curve are calculated from the recordings of T.C.C 1 using one dimensional Fourier's conduction equation. The heat flux is computed from the total power input to heaters through the two controllers. For comparison, a transient boiling curve by quenching under the same flow conditions is constructed[4] and plotted in Fig. 2. Good agreement is observed between these boiling curves in the film and transition boiling régimes. However, it is noticed that the transient boiling curve in the nucleate régime is shifted to the higher wall temperature side. This is due to bubble clouding on the heated surface during quenching experiments thus retarding boiling heat transfer process [5].

The arrangement in using the proportional controller to regulate the power input into the inner array of heaters is very crucial in maintaining a stable control in the transition boiling régime. In that régime, the heat transfer process is highly unstable -- heat transfer modes occur alternately between film and nucleate boiling -- thus causing wall temperatures to oscillate rapidly. Although it has been damped out considerably by the time it reaches the temperature sensor location, T.C.C 2, still, the proportional controller provides the only effective means in controlling these oscillating temperatures. This is because the proportional controller is capable of fine tuning, i.e. it can provide rapidly a continuing and varying power input into heaters in proportion to the deviation between the set-point temperature and the sensor temperature.

Conclusion

A method to measure an entire flow boiling curve under steady state condition has been proposed. The measured steady state data are compared favorably with transient results, especially in film and transition boiling régimes.

Acknowledgements

Financial support from the U.S. Nuclear Regulatory Commission is acknowledged. The authors also wish to express thanks to Messrs. H. Ragheb and S. Roy for providing the transient boiling data.

References

1. S.C. Cheng, W.W.L. Ng, K.T. Heng and H. Ragheb, "Transition Boiling Heat Transfer in Forced Vertical Flow", Final Report (1976-77), Argonne contract No. 31-109-38-3564 (1977).

2. S.C. Cheng, W.W.L. Ng, K.T. Heng and D.C. Groeneveld, "Measurements of Transition Boiling Data for Water Under Forced Convective Conditions", J. Heat Transfer, 100, 382 (1978).

3. S.C. Cheng, W.W.L. Ng and K.T. Heng, "Measurements of Boiling Curves of Subcooled Water Under Forced Convective Conditions", Int. J. Heat Mass Transfer (in press).

4. S.C. Cheng, H. Ragheb, W.W.L. Ng, K.T. Heng and S. Roy, "Transition Boiling Heat Transfer in Forced Vertical Flow", Final Report (1977-78), Argonne contract No. 31-109-38-3564 (1978).

5. A.E. Bergles and W.G. Thompson, Jr., "The Relationship of Quench Data to Steady-State Pool Boiling Data", Int. J. Heat Mass Transfer, 13, 55 (1970).

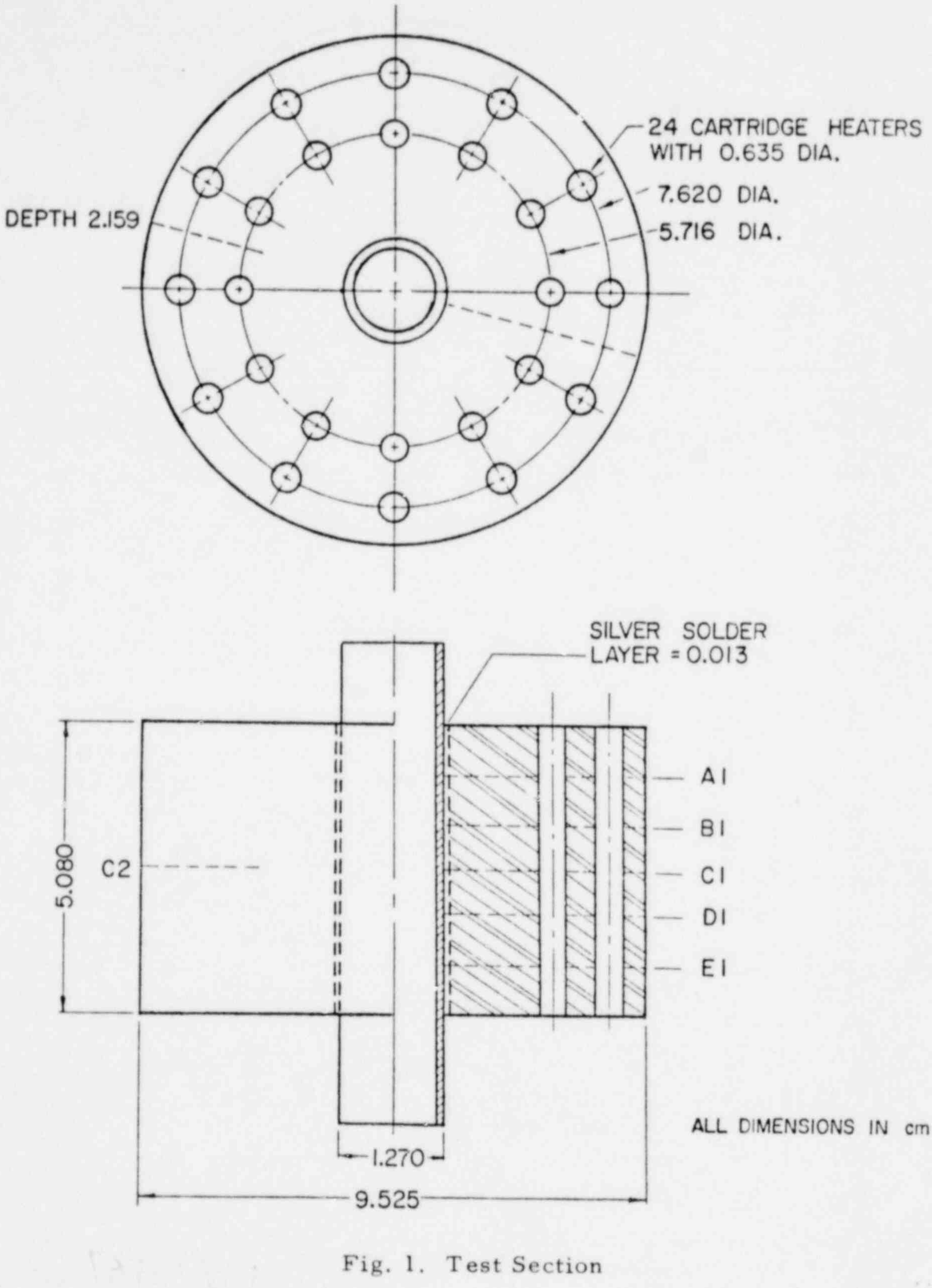

Fig. 1. Test Section

1372 168

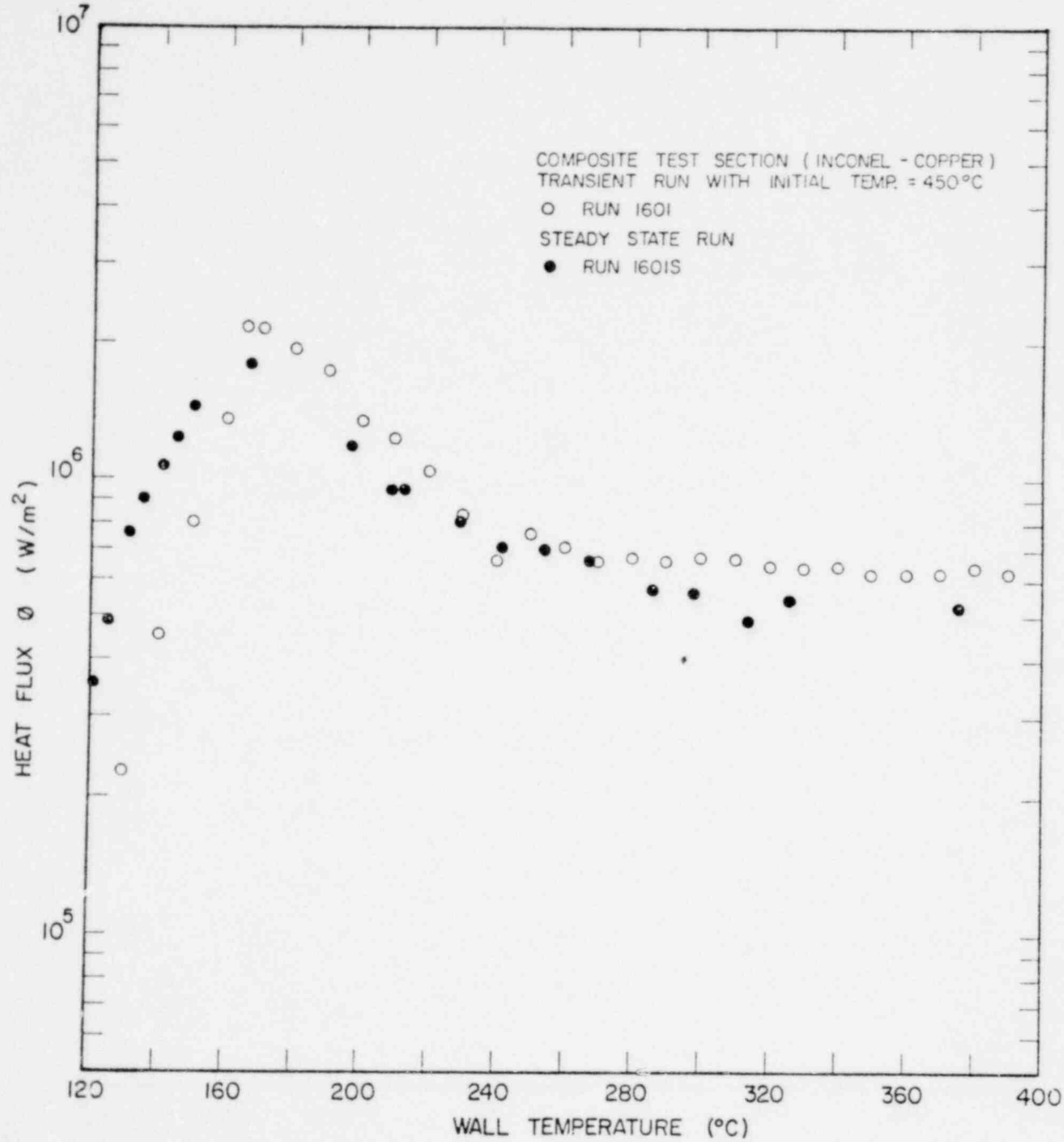

Fig. 2. Boiling Curves of Distilled Water for G = 136 kg/m^{2}s and ΔT_{sub} = 13.9°C

APPENDIX II

Surface Wetted Area During Transition Boiling in Forced Convective Flow

. 1372 170

SURFACE WETTED AREA DURING TRANSITION BOILING IN FORCED CONVECTIVE FLOW

H. S. Ragheb and S. C. Cheng
Department of Mechanical Engineering
University of Ottawa, Ottawa, Canada

Introduction

During a loss-of-coolant accident (LOCA) in a water cooled nuclear reactor, some portions of the core are under the transition boiling heat transfer mode. The transition boiling mode is most efficient at its lower temperature boundary which corresponds to the critical heat flux (CHF). Immediately after CHF, the heated surface can no longer support the continuous liquid contact, and heat transfer deteriorates due to the increase of area covered by dry patches.

The heated surface during transition boiling is partially wet and partially covered by vapor. Hence a convenient way to deal with transition boiling is to assume that it is a combination of both unstable nucleate boiling and unstable film boiling alternately existing at any given location at the heated surface. The variation of heat transfer rate with temperature is primarily a result of the change in the fraction of time that each boiling mode exists at a given location as stated by Berenson [1].

Following Berenson's description of the transition boiling mode, Kalinin et al [2] weighted the two heat transfer components (nucleate

1372 171

and film boiling) by f_k, the fraction of surface that is wet. The total heat flux q_t is then expressed as

$$q_t = q_{NB} f_k + q_{FB}(1 - f_k) \tag{1}$$

and
$$f_k = \frac{q_t - q_{FB}}{q_{NB} - q_{FB}} \tag{2}$$

where q_{NB} and q_{FB} represent nucleate boiling and film boiling, respectively, assuming that both expressions can be extrapolated into the transition boiling régime. Knowing q_{NB} and q_{FB} from correlations, and using experimental data of q_t, one can obtain the expression of f_k in terms of T_w, wall temperature, T_{max}, wall temperature at maximum heat flux, and T_{min}, wall temperature at minimum heat flux. Kalinin et al. obtained two functions for f_k, one being exponential decay with increasing T_w.

Tong and Young [3] suggested that the total heat flux q_t is a sum of two components, i.e.

$$q_t = q_{TB} + q_{FB} \tag{3}$$

where q_{TB} is the transition boiling component which decays with increasing T_w (see Fig. 4). They obtained an empirical, exponential decay expression for q_{TB} in terms of T_w and x, quality. Hsu and Graham [4] related this expression to the fraction of wetted area. Recently, Tong [5] suggested that the wetted area fraction can be related to q_{TB} by

$$f_T = q_{TB}/q_{NB} \tag{4}$$

where q_{NB} can be approximated by q_{CHF} in the transition boiling regime.

The purpose of this study is (a) to examine the measurements of the wetted area during a quenching process using an electric probe, and (b) to compare these measurements with the predictions of Kalinin and Tong. The study involving the electric probe in detecting the phase change on a heated surface has been reported in [6,7].

Experimental Apparatus

Fig. 1 shows schematically the configuration of the probe. The probe made of zirconium wire coated by a platinum tip is suited for high temperature operation. It can detect the presence of liquid droplets contact on the heated surface by measuring voltage drop between the platinum tip (as one electrode) and the heating surface (as another electrode). The test section with the probe and the adjacent thermocouple is shown in Fig. 2. Tests were conducted for water at atmospheric pressure under flow boiling conditions with G, mass flux, varying from 34-102 kg/m^2s and ΔT_{sub}, inlet subcooling, varying from 0-28^oC. Further details of the experimental apparatus and procedures may be found in [6,7].

Results and Discussion

Fig. 3 shows an example of the probe signal and the adjacent thermocouple signal for a typical rewetting run. The region BC characterizes the transition boiling mode where the wetted area increases with time. The boiling curve constructed as shown in Fig. 4 was based on the temperature-time trace of the thermocouple (Fig. 3) using the technique developed in [8].

For a typical point in the transition boiling, the quantities of q_t, q_{NB} and q_{FB} defined in the Kalinin's approach are illustrated in Fig. 4. q_{NB} has been extrapolated to T_{min} and q_{FB} to T_{max}. The extrapolation of q_{FB} in this case being a horizontal line is due to the fact that film boiling is almost independent of wall superheat under the present flow conditions [9-11], q_{TB} defined by Tong and Young is also indicated in the figure.

The predicted fraction of wetted area using Eqs. (2) and (4) based on the boiling curve of Fig. 4 is shown in Fig. 5. The measured fraction of wetted area by the probe is also presented in Fig. 5 for comparison. This is obtained from Fig. 3 by assuming $f = 1$ at CHF and $f = 0$ at the minimum heat flux (to be explained later), the points (as a function of time), in between are read directly from the graph. Since the time coordinate is related to T_w in the data reduction process, thus f vs T_w can be obtained as shown. In general, both measured and predicted results display a same exponential trend (which becomes a straight line in a semi-log plot). The predicted wetted area, using Tong's expression, is in closer agreement with the probe measurement, except at CHF. As seen from Figs. 3 and 4, (a) the onset of intermittent wetting at point B is very close to the minimum heat flux, hence it can be assumed $f = 0$ at the minimum heat flux, and (b) the onset of continuous liquid contact at point C coincides with the CHF point, and furthermore, point C approaches the mean value of voltage drop from the nucleate boiling side (continuous liquid contact) as indicated in Fig. 3, thus $f = 1$ can be assumed at CHF.

1372 174

The agreement between the probe measurement and Tong's expression suggests a new method of predicting transition boiling. If q_{CHF} and q_{FB} are given, and with the measured fraction of wetted area by the probe, transition boiling can be calculated from Eqs. (3) and (4).

Conclusions

1. The fraction of wetted area predicted using Tong's expression in transition boiling under flow conditions compares favorably with the probe measurement.
2. Transition boiling under flow conditions can be predicted if (a) q_{CHF} and q_{FB} are given, and (b) the measured fraction of wetted area from the probe is available.
3. This study provides some insight of transition boiling phenomenon through the measurement of the fraction of wetted area. It is hoped that this will lead to improved modelling of the transition boiling process.

Acknowledgement

Financial support from the U.S. Nuclear Regulatory Commission is acknowledged.

References

1. Berenson, P.J. "Experiments in Pool-Boiling Heat Transfer", Int. J. of Heat and Mass Transfer, Vol. 5, 1962, pp. 985-999.

2. Kalinin, E.K., Berlin, I.I., Kostyuk, V.V., and Nosova, E.M. "Heat Transfer in Transition Boiling of Cryogenic Liquids", Proceedings, Cryogenics Engineering Conference, Queen's University, Kingston, Ontario, Canada, 1975, pp. 273-277.

3. Tong, L.S., and Young, J.D. "A Phenomenological Transition and Film Boiling Heat Transfer Correlation", Proc. of the 5th Int. Heat Transfer Conference, Vol. IV, Tokyo, Japan, 1974, pp. 120-124.

4. Hsu, Y.Y. and Graham, R.W., Transport Processes in Boiling and Two-Phase Systems, McGraw-Hill, 1976, pp. 254-256.

5. Tong, L.S. "Heat Transfer in Reactor Safety", Proceedings, 6th Int. Heat Transfer Conference, Vol. 6, Toronto, Canada, 1978, p. 296.

6. Ragheb, H.S., Cheng, S.C., and Groeneveld, D.C. "Measurement of Transition Boiling Boundaries in Forced Convective Flow", Int. J. of Heat and Mass Transfer (in press).

7. Ragheb, H.S., "Development of Electric Probes to Detect Phase Change at a Heated Surface", M.A.Sc. Thesis, Univ. of Ottawa, 1977.

8. Cheng, S.C., Heng, K.T., and Ng, W., "A Technique to Construct a Boiling Curve from Quenching Data Considering Heat Loss", Int. J. of Multiphase Flow, Vol. 3, 1977, pp. 495-499.

9. Cheng, S.C., Ng, W., Heng, K.T. and Groeneveld, D.C., "Measurements of Transition Boiling Data Under Forced Convective Conditions", J. of Heat Transfer, Vol. 100, 1978, pp. 382-384.

10. Fung, K.K., "Forced Convective Transition Boiling", M.A.Sc. Thesis, Dept. of Mechanical Engineering, University of Toronto, 1976.

11. Newbold, F.J., Ralph, J.C., and Ward, J.A., "Post-Dryout Heat Transfer Under Low Flow and Low Quality Conditions", AERE-R8390, 1976.

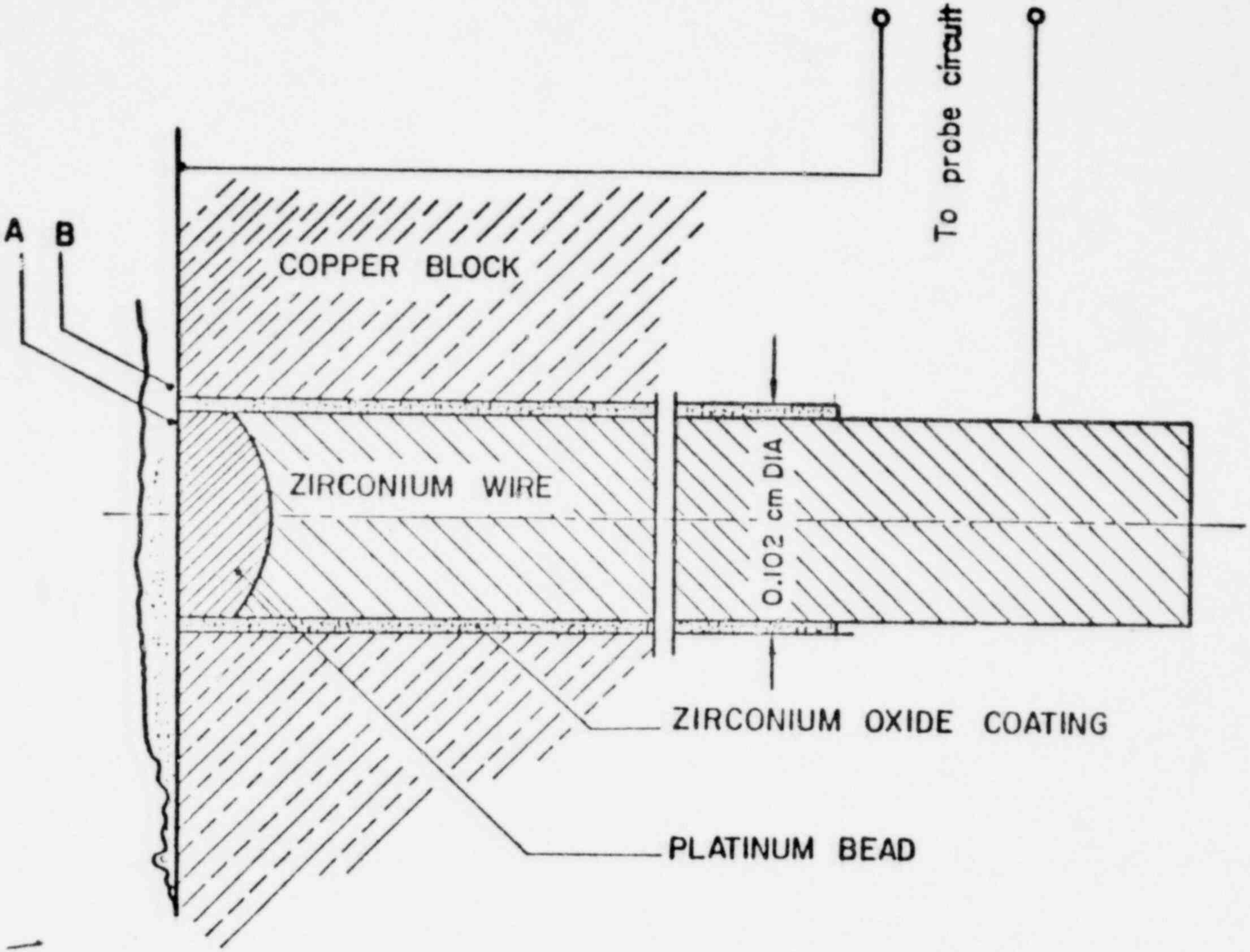

Fig. 1. Probe Configuration

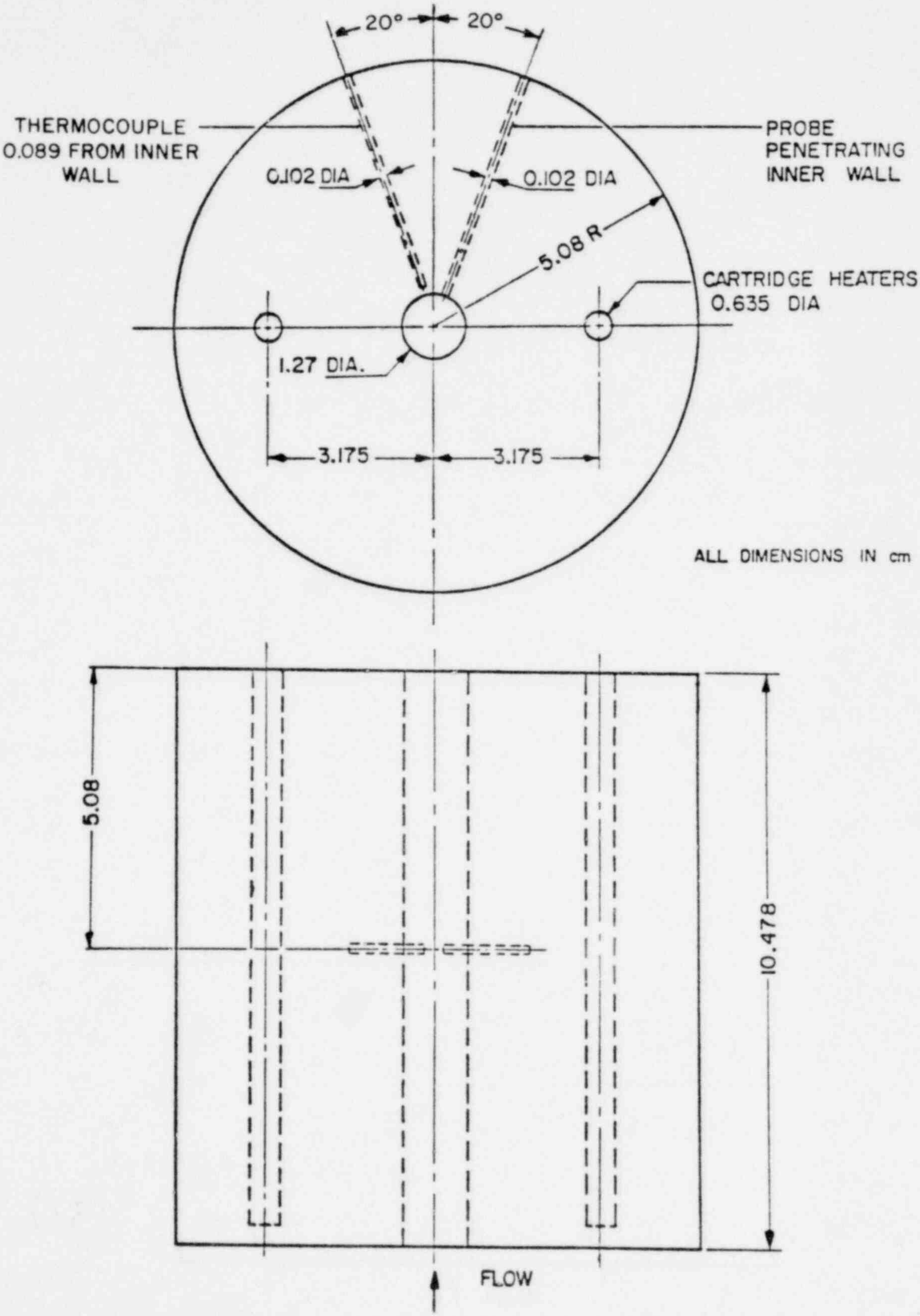

Fig. 2. Test Section

1372 178

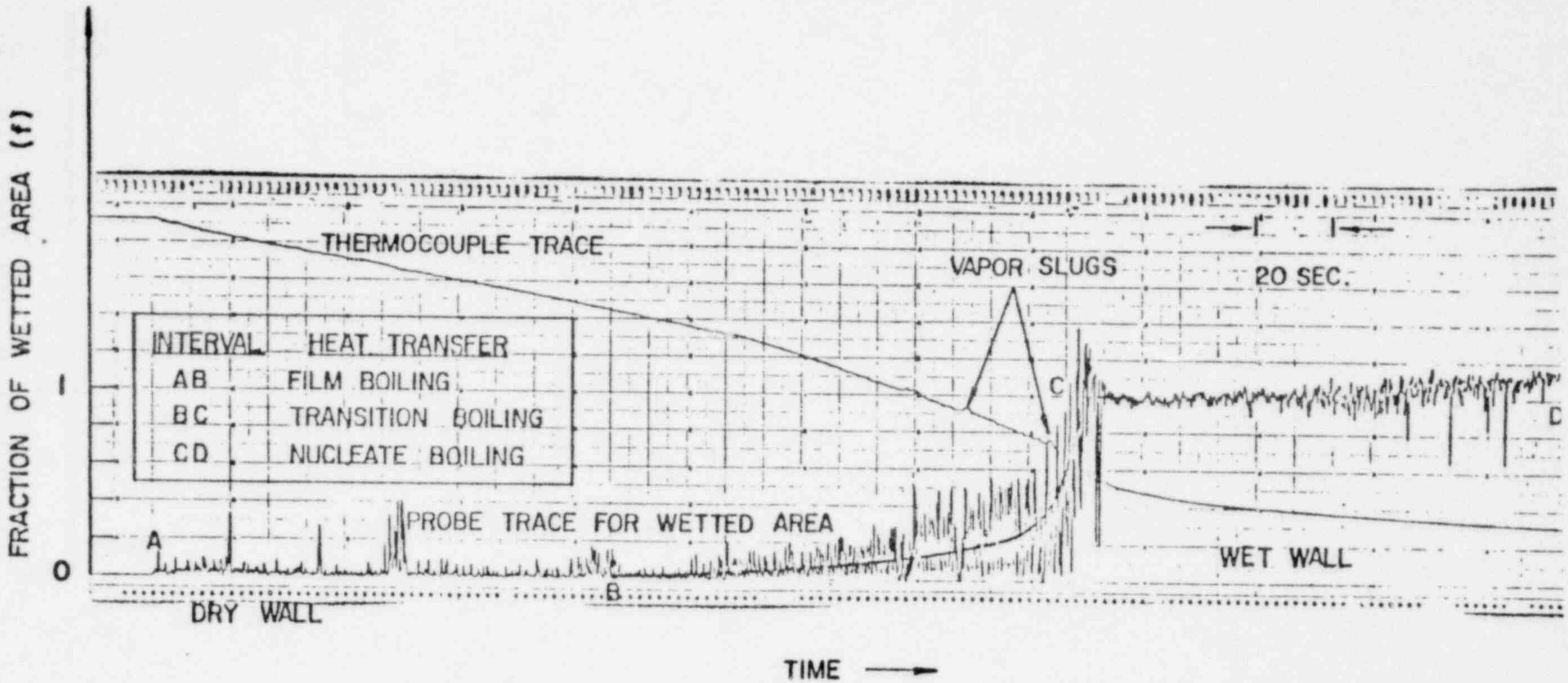

Fig. 3. Signals Recorded from the Probe and the Thermocouple in Flow Boiling

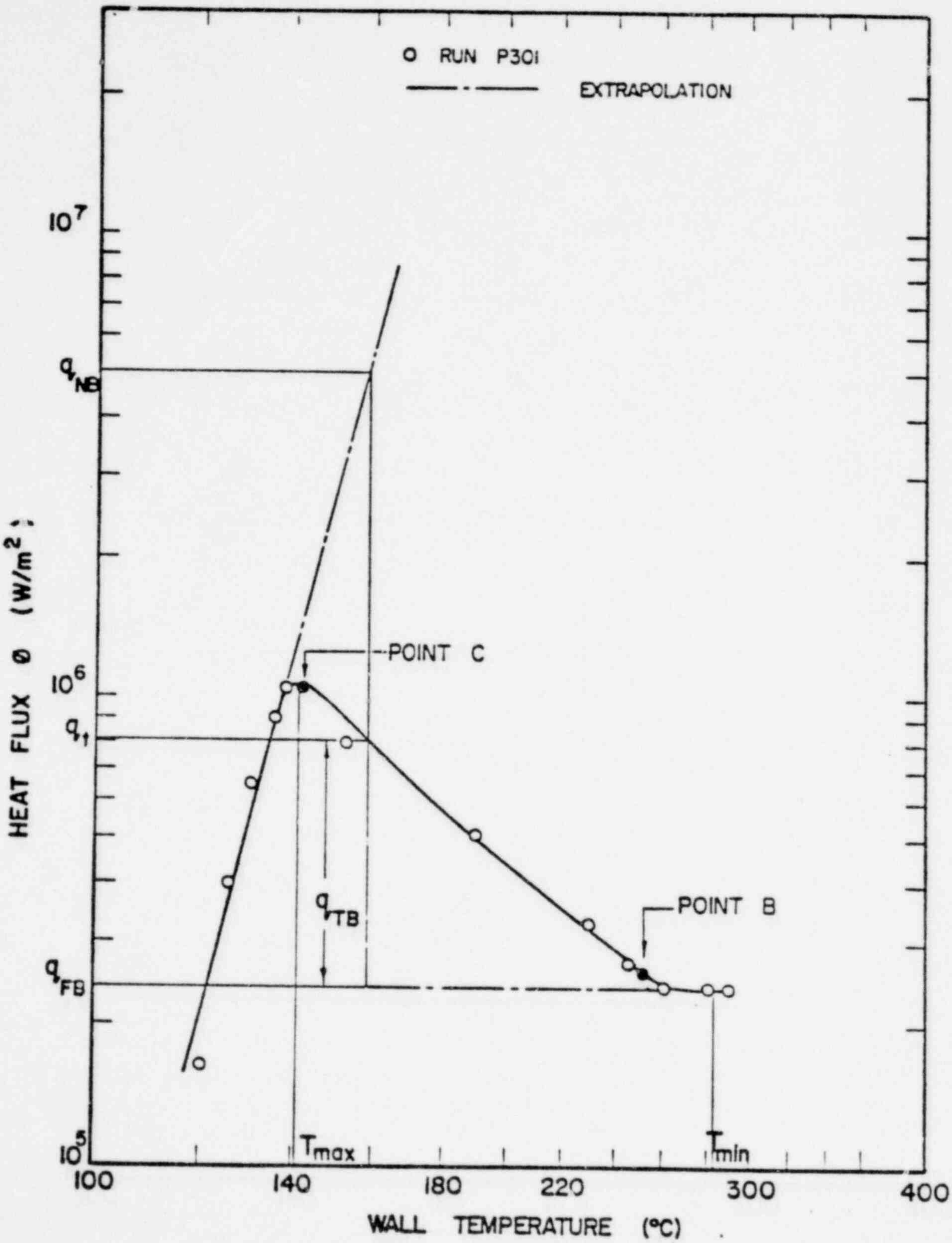

Fig. 4. Boiling Curve of Water for $G = 68\ kg/m^2s$ and $\Delta T_{sub} = 27.8°C$

. 1372 180

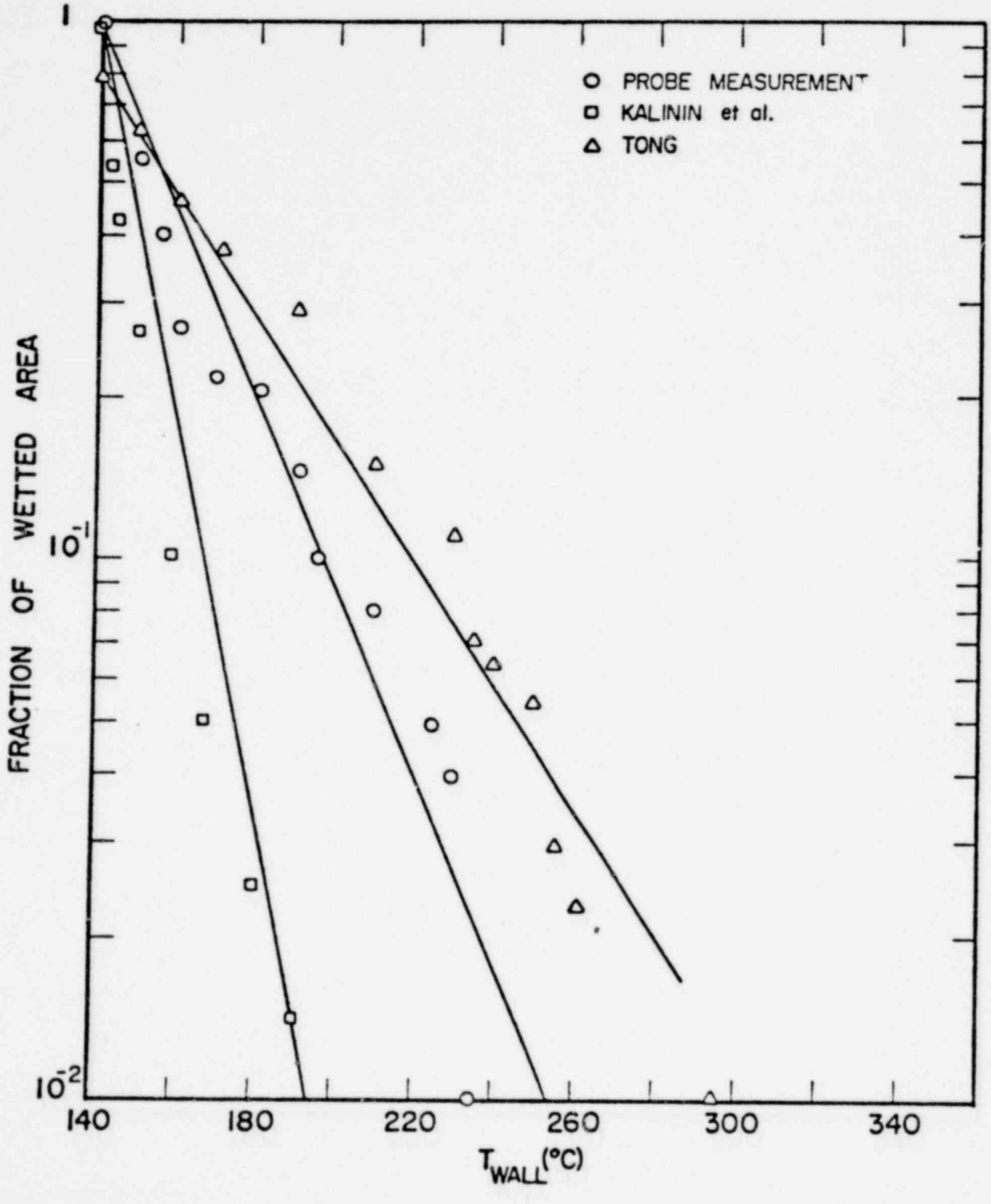

Fig. 5. Comparison of Measured and Predicted Fraction of Wetted Area

1372 181

Distribution for NUREG/CR-1054 (ANL-,9-78)

Internal:

J. A. Kyger
J. W. Boudrot
R. Avery
H. K. Fauske
E. Taylor (3)
P. A. Lottes (32)
R. E. Henry
J. C Leung
A. B. Krisciunas
ANL Contract File
ANL Libraries (3)
TIS Files (4)

External:

NRC, for distribution per R2 (320)
DOE-TIC (2)
Manager, Chicago Operations and Regional Office, DOE
Chief, Office of Patent Counsel, DOE-CORO
President, Argonne Universities Association, Argonne, Illinois
Reactor Analysis and Safety Division Review Committee:
- S. Baron, Burns and Roe, Inc., 700 Kinderkamack Rd., Oradell, N.J. 07649
- J. R. Dietrich, Combustion Engineering, Inc., 1000 Prospect Hill Rd., Windsor, Conn. 06095
- W. Kerr, Dept. of Nuclear Engineering, University of Michigan, Ann Arbor, Mich. 48105
- M. Levenson, Electric Power Research Institute, 3412 Hillview Ave., Palo Alto, Calif. 94304
- S. Levy, S. Levy Inc., 1901 S. Bascom Ave., Campbell, Calif. 95008
- D. Okrent, Energy and Kinetics Dept., University of California, Los Angeles, Calif. 90024
- N. C. Rasmussen, Dept. of Nuclear Engineering, Massachusetts Institute of Technology, Cambridge, Mass. 02139